NASA Contractor Report 195452

Robust Integration Schemes for Generalized Viscoplasticity With Internal-State Variables

Part I Theoretical Developments and Applications

Atef F. Saleeb and Wei Li
University of Akron
Akron, Ohio

May 1995

Prepared for
Lewis Research Center
Under Grant NAG3–1493

National Aeronautics and
Space Administration

Robust Integration Schemes for Generalized Viscoplasticity with Internal-State Variables; Part I Theoretical Developments and Applications

Atef F. Saleeb, Professor
Wei Li, Graduate Research Assistant
Department of Civil Engineering
University of Akron
Akron, Ohio 44325-3905

Prepared for
Lewis Research Center
Under Grant NAG3-1493-ONR

Acknowledgments

This work was completed as part of a research project supported by NASA-Lewis Grant No. NAG3-1493-ONR. We would like to acknowledge the encouragement, technical, and financial support provided by R. Ellis and S. M. Arnold of the structural fatigue Branch at NASA Lewis during the course of this project. Special thanks are also due to S. M. Arnold and T. E. Wilt for their assistance, many helpful discussions, and review comments, in the final preparation of these reports.

ABSTRACT

This two-part report is concerned with the development of a general framework for the implicit time-stepping integrators for the flow and evolution equations in generalized viscoplastic models. The primary goal is to present a complete theoretical formulation, and to address in detail the algorithmic and numerical analysis aspects involved in its finite element implementation, as well as to critically assess the numerical performance of the developed schemes in a comprehensive set of test cases. On the theoretical side, the general framework is developed on the basis of the unconditionally-stable, backward-Euler difference scheme as a starting point. Its mathematical structure is of sufficient generality to allow a unified treatment of different classes of viscoplastic models with internal variables. In particular, two specific models of this type, which are representatives of the present state-of-art in metal viscoplasticity, are considered in applications reported here; i.e., fully associative (GVIPS) and non-associative (NAV) models. The matrix forms developed for both these models are directly applicable for both initially isotropic and anisotropic materials, in general (three-dimensional) situations as well as subspace applications (i.e., plane stress/strain, axisymmetric, generalized plane stress in shells). On the computational side, issues related to efficiency and robustness are emphasized in developing the (local) iterative algorithm. In particular, closed-form expressions for residual vectors and (consistent) material tangent stiffness arrays are given explicitly for both GVIPS and NAV models, with their maximum sizes "optimized" to depend only on the number of independent stress components (but independent of the number of viscoplastic internal state parameters). Significant robustness of the local iterative solution is provided by complementing the basic Newton-Raphson scheme with a line-search strategy for convergence. In the present first part of the report, we focus on the theoretical developments, and discussions of the results of numerical-performance studies using the integration schemes for GVIPS and NAV models.

Robust Integration Schemes for Generalized Viscoplasticity with Internal-State Variables; Part I Theoretical Developments and Applications

1. Introduction and Literature Review

Dealing with the general topic of computational inelasticity, the scope of the work in this report is focused on the development of algorithms for the integration of rate dependent constitutive equations. In recent years, this subject has attracted considerable attention and will form the basis for the present work. In particular, recent literature has clearly emphasized the use of implicit integration schemes in view of their robustness; i.e., their superior stability and convergence properties for viscoplasticity, as well as for the limiting case of inviscid plasticity.

In regards to the rate dependent constitutive models, a number of viscoplastic models were developed to represent the material behavior of metals and composites, etc. All viscoplastic models can be classified into two classes, the first is the fully associative viscoplastic model, or GVIPS (Generalized Viscoplastic with Potential Structure), the second is the NAV (Non-associative Viscoplastic models). GVIPS possess both the thermodynamic potential (Gibb's function) and the dissipation function (Ω form), while NAV generally refer to those models that have partially (e.g., Ω form only) or totally incomplete potential form. In these latter NAV models, thermodynamics requirements are simply reduced to the fundamental dissipation inequality only. For these two different classes of models, a general computational framework suitable for implementation of both is needed, and this constitutives the major part in the developments reported here.

1.1 Integration Schemes

Computational algorithms for the integration of constitutive relations play a central role in the inelastic finite element analysis of engineering structures. For example, because of their

simplicity, the classical von Mises (or J_2-type) theories of inviscid plasticity [28], and generalizations for its time-dependent viscoplastic counterpart [37, 58] are extensively utilized for *isotropic* metals. Correspondingly, a major research effort has been devoted over the years to the development and critical assessment of stress updating or integration schemes for the rate equations in these material models [2, 8, 12-14, 16, 22, 29, 31, 33-35, 40, 42, 44-45, 48-49, 52, 54, 57, 63, 67-70, 74, 76-78, 80]. As a result, several powerful techniques are currently available; e.g. refer to the extensive reviews and evaluations in [51, 64] for plasticity and [2, 30, 35, 65, 78] for viscoplasticity.

In particular, note that, in early applications the explicit integration schemes (i.e., forward Euler method) were predominate because of their ease in implementation, and because they do not require evaluating and inverting a Jacobian matrix. However, explicit integrators may not be efficient. That is, too many iteration steps may be required and convergence stability can not be guaranteed [49, 54, 80]. More recent work has clearly emphasized the use of *implicit* integration methods [12-14, 22, 29, 31, 33, 40, 42, 45, 48, 52, 57, 63, 65, 68-69, 74, 76-77] in view of their superior stability and convergence properties [30, 51]. Several alternative approaches have been used in the derivation and subsequent mathematical analyses of these latter methods (collectively known as return mapping algorithms in recent computational-plasticity literature). For instance, these include convex analysis techniques for variational inequalities of plasticity [23, 32, 46, 50], mathematical programming or holonomic methods for incrementally external paths [11, 18, 41, 43], the "substructure" analogy [59], asymptotic expansions for integral-equations in viscoplasticity [17, 25, 75], as well as the more conventional finite differencing schemes [26] and their generalizations; i.e., in the form of semi-implicit or forward gradient approach [e.g. 2, 57, 78], and also implicit trapezoidal or midpoint rules [30, 51, 64]. Walker's asymptotic integration scheme is of more recent origin, and exhibits a number of unique advantages which are marked improvement in accuracy and stability over existing integration algorithms for the case of isotropic materials subjected to uniaxial loads [17, 75]. In these references, the asymptotic integrator is described for dissipative linear two dimensional systems of ordinary

differential equations, and is shown to yield the exact solution for a one dimensional linear equation. However, recent work shows that for higher dimensional systems of nonlinear equations, such as Freed's viscoplastic model, accuracy and stability cannot be guaranteed in general [27]. From the standpoint of practical applications, the one-step, fully implicit, backward Euler scheme is presently one of the most widely used integrators [14, 29-31, 33, 40, 48, 51-52, 63-64, 68-69, 76-77]. For the computationally intensive viscoplastic applications, found in typical finite element analysis, implicit backward Euler integration methods have become the proven standard for the numerical integration of the viscoplastic rate equations [27, 65].

1.2 Viscoplastic Models

During the past decade, much progress has been made in the development of viscoplastic constitutive equations. Several viscoplastic models have been proposed and developed to treat the complex time dependent viscoplastic behavior of metals, alloys and composites at high temperature [15, 24, 60, 62]. The deformation behavior of materials at high temperature involves energy dissipation and material stiffness variations due to physical changes in the material's microstructure. Consequently, thermodynamic arguments have often been utilized as a foundation on which phenomenological constitutive laws may be formulated. The general form for a fully-associative potential-based viscoplastic formulation in terms of the Gibb's thermodynamic potential has been put forth in [3-5]. The complete potential-based class of inelastic constitutive models exhibit a number of unique advantages from both a theoretical and a computational standpoint, for example, the symmetry of the resulting consistent tangent stiffness matrix, and possesses a form which is convenient for further development of new deformation and damage models. These advantages serve to motivate further development and use of this class of models.

Another class of constitutive models are those that are nonassociative and are currently used by industry, e.g., the unified viscoplastic theory of Robinson and Duffy [60,62] for metal matrix composites at high temperature, together with its extension for coupled creep-damage analysis in [61]; and Freed's viscoplastic model with creep and plasticity bounds to analyze the response of polycrystalline metals at high temperature [24]. Recent work has demonstrated that the above models may be modified to restore the complete potential structure. With regards to the computational algorithms, research work for the more complex constitutive theories is still needed. In this regard, the study of the important issues involved in such an undertaking constitutes our main objective in the present report.

2. Scope, Objectives and Contribution

2.1 Scope

From the standpoint of practical applications of interest (i.e., large-scale numerical simulations), and in view of the above discussion, the focus of the present work is on the stress updating schemes of the one-step, fully implicit, backward Euler difference scheme. This is the simplest in its class, and is certainly the most widely used at present. Based on recent experience and results, this scheme was found to be efficient and stable when effectively utilized in a class of isotropic and anisotropic coupled viscoplastic-damage models.

With regards to the constitutive models employed, two general classes of unified viscoplastic theories are considered:

(a) The nonassociative models (NAV)
(b) The fully associative, or complete potential-based, models (GVIPS)

Both of these models are sufficiently general for the anticipated applications; i.e., incorporating such important response characteristics as nonlinear (isotropic and/or kinematic) hardening, various recovery mechanisms, etc., and both are amenable to extensions for nonisothermal conditions, as well as anisotropy (i.e., generalized J_2 format). The majority of viscoplasticity models currently in use (at NASA and elsewhere) belong to class (a). Several developments in class (b) are currently underway as these models are very appealing in view of their theoretically sound basis from the thermodynamics standpoint, and the symmetries exhibited in the corresponding integrated forms of their flow and evolution equations. This report will discuss the present implementation which has been developed in terms of a framework which is applicable to both GVIPS and nonassociative models to show the robustness of the backward Euler integration algorithm. As an example of a nonassociative model, Freed's model [24] was chosen for implementation into the proposed integration algorithm. For the generalized form of GVIPS, the decoupled potential framework is assumed and the specific GVIPS model is put forth.

For conciseness, the discussion is limited to a case involving small deformations (in which the initial state is assumed to be stress free throughout), an initially isotropic material, and isothermal conditions. Note that the implementation framework is also valid for an anisotropic material.

2.2 Objectives

For each of the viscoplastic models considered, and the associated implicit backward Euler integration method, the following tasks are to be completed:

(1) Detailed study of the underlying mathematical structure of the viscoplastic equations, and the corresponding integrated fields of stress and internal state variables.

(2) Development and implementation of the stress-updating algorithm, and associated line search and subincrementing schemes.

(3) Testing of the convergence, stability, and accuracy properties of the algorithms.

(4) Documentation of results, guidelines, and recommendations for effective utilization of the schemes developed.

Our primary objective in item (1) is to identify the pertinent matrix operators needed in the algorithmic development; i.e., concise forms of the integrated field equations, and convergence limits for the subincrementing control strategy in item (2). The implementation in item (2) will encompass several nonlinear solution procedures; i.e., both the initial (constant) and tangent (variable) stiffness formats. The latter utilizes appropriate forms of the consistently-derived material tangent stiffness; i.e., model/integrator-dependent.

The implementation and coding in (2) will be written in a "modular", "stand-alone", format with full documentation of the associated material-model subroutines. This will facilitate a straightforward utilization of the developed algorithms in other nonlinear finite element analysis codes.

In conjunction with (3), an extensive number of discriminating test problems will be utilized. The objective is to enable firm conclusions to be made regarding the "relative" merits and/or limitations of various schemes.

2.3 Contribution

Based on the present work, some achievements are summarized as follows:

(1) Original equations of Freed's model are recast into the matrix format described in [65] to facilitate the model's implementation into the newly developed frame-work discussed in Part II [38] of this work.

(2) Freed's nonassociative model is implemented successfully in finite element analysis for the generalized plane stress case.

(3) The algorithm described in the report is proven to be accurate and efficient. Convergence and stability are guaranteed.

(4) Line search technique is used successfully to achieve robustness of the integration scheme.

3. Mathematical Formulations of Viscoplastic Models

3.1 Introduction

In this section, mathematical formulations of the complete potential-based viscoplastic structure is discussed. Based on recent work [3, 5], the general form for GVIPS should have two key ingredients; 1). the thermodynamic potential, or Gibb's function (or conjugate free energy, Helmholtz function) defining the equations of state, and 2). the viscoplastic dissipation function (Ω form) for the ensuing flow and evolution laws of inelastic strain and internal state parameters. The previous forms typically employed by many researchers [60, 62, 24] in discussing the general structure of the "thermodynamically based" constitutive equations are Ω-form (flow or dissipation potential). These forms are introduced solely for convenience in satisfying the thermodynamic admissibility restriction of the engineering materials based on simple properties of non-negativeness and convexity of these functions. From a strict mathematical standpoint, the "thermodynamic-admissibility" restriction associated with the dissipative mechanisms reduce to the well-known Clausius-Duhem or dissipative inequality (Ω-form) [19, 39]. However, such Ω-forms do not presuppose or automatically imply the existence of the total (integrated) forms of the associated thermodynamic potentials, e.g., the (Helmholtz) free energy, or Gibb's function. Together, the Ω-form and the a priori assumption for the existence of Gibbs and Helmholtz functions will lead to a complete potential-based formulation. For distinction, the original model, i.e., using only the Ω-forms, is referred to as the incomplete potential formulation or the so-called nonassociative model.

The complete potential-based class of inelastic constitutive equations possess a number of distinct and important attributes from both a theoretical and a computational standpoint. First, they constitute the cornerstone of numerous regularity properties and bounding (or limit) theorems in plasticity and viscoplasticity. Second, they result in a sufficiently general variational structure, whose properties can be exploited to derive a number of useful material conservation laws. Third, on the numerical side, the discrete form of this same variational structure is of great advantage in the development of efficient algorithms for finite element implementation, for example, symmetry-preserving material tangent stiffness operators are easily obtained in implicit solution schemes (examples are given later in Part II of this report). Finally, this complete potential-based framework conveniently lends itself to intelligent application of symbolic manipulation systems that facilitate the construction, implementation, and analysis of new deformation and damage models [3]. Several of the currently used forms [60, 62, 24] do not conform to the general potential framework, but it is still possible in some cases, by modifications of the employed forms, to restore the complete potential structure.

3.2 Generalized Viscoplasticity With Potential Structure (GVIPS)

The discussion is limited to the case of small deformations, in which the initial state is assumed to be stress-free throughout. For generality, the initial state of material isotropy or anisotropy is left unspecified in this section; i.e., except for the explicit appearance of the corresponding material-directionality tensors in the arguments list for the potential functions employed, all derivations remain generally applicable.

Consider the following general form for the Gibb's potential:

$$\Psi = \Psi (\sigma_{ij}, \alpha_T^b, D^d) \qquad (3.1)$$

where α_T^b denotes the T th-order tensorial internal state variables (where b=1,...,n_b ; T= 1,...,n_T), α_T^b can be a second-order tensor (back stress) or higher order tensors, b denotes

the number of tensorial internal state variables; D^d is the scalar internal state variable (where d=1,...,n_d) and σ_{ij} the cauchy stress tensor. This is a typical general form for the Gibb's potential, in which as many internal variables as desired may be specified in eq. (3.1). The potential may be decoupled into elastic and inelastic parts:

$$\Psi = \Psi^e(\sigma_{ij}) + \Psi^i(\alpha_T^b, D^d) \tag{3.2}$$

or

$$\Psi = \Psi^e(\sigma_{ij}) + \sum_{b=1}^{n_b} \Psi_\alpha^i(\alpha_T^b) + \sum_{d=1}^{n_d} \Psi_D^i(D^d) \tag{3.3}$$

It follows from eq. (3.3) then that:

$$\varepsilon_{ij} - \varepsilon_{ij}^p = \frac{\partial \Psi}{\partial \sigma_{ij}} \tag{3.4}$$

$$\gamma_T^b = \frac{\partial \Psi}{\partial \alpha_T^b} \tag{3.5}$$

$$\gamma_D^d = \frac{\partial \Psi}{\partial D^d} \tag{3.6}$$

where ε_{ij} is the total strain and ε_{ij}^p is inelastic strain tensor, respectively.

These above relations are defined as the equations of state, and σ_{ij}, α_T^b, D^d are the "force-like" thermodynamic state variables while ε_{ij}, γ_T^b, γ_D^d are the conjugate "displacement-like" variables (affinities).

Now, assume the existence of a dissipation potential of the form,

$$\Omega = \Omega(\sigma_{ij}, \alpha_T^b, D^d) \tag{3.7}$$

Which when written in its decoupled form [3] gives,

$$\Omega = \Omega_1(\sigma_{ij}) + \sum_{b}^{n_b} \Omega_2^b(\alpha_T^b) + \sum_{d}^{n_d} \Omega_3^d(D^d) \tag{3.8}$$

In order to provide a framework for the definition of the inelastic strain rate ($\dot{\varepsilon}_{ij}^p$) and ensure its thermodynamic admissibility, the Clausius-Duhem or dissipation inequality is required. That is,

$$\Omega(\sigma_{ij}, \alpha_T^b, \mathrm{D}^d) = \sigma_{ij}\dot{\varepsilon}_{ij}^p + \sum_{b}^{n_b}(\alpha_T^b \dot{\gamma}_T^b) + \sum_{d}^{n_d}(D^d \dot{\gamma}_D^d) \geq 0 \tag{3.9}$$

The rate of change of the affinities may then be expressed in terms of their corresponding internal state variables. That is, the flow or kinetic law becomes:

$$\dot{\varepsilon}_{ij}^p = \frac{\partial \Omega}{\partial \sigma_{ij}} \tag{3.10}$$

$$\dot{\gamma}_T^b = \frac{\partial \Omega}{\partial \alpha_T^b} \tag{3.11}$$

$$\dot{\gamma}_D^d = \frac{\partial \Omega}{\partial D^d} \tag{3.12}$$

From eqs. (3.5) and (3.6),

$$\dot{\gamma}_T^b = \frac{d}{dt}\left[\frac{\partial \Psi}{\partial \alpha_T^b}\right] = \frac{\partial^2 \Psi}{\partial \alpha_T^b \partial \alpha_T^b}\dot{\alpha}_T^b \tag{3.13}$$

$$\dot{\gamma}_D^d = \frac{d}{dt}\left[\frac{\partial \Psi}{\partial D^d}\right] = \frac{\partial^2 \Psi}{\partial D^d \partial D^d}\dot{D}^d \tag{3.14}$$

then, from eqs. (3.11) (3.12) (3.13) (3.14),

$$\dot{\alpha}_T^b = [\frac{\partial^2 \Psi}{\partial \alpha_T^b \partial \alpha_T^b}]^{-1} \dot{\gamma}_T^b = [\frac{\partial^2 \Psi}{\partial \alpha_T^b \partial \alpha_T^b}]^{-1} \frac{\partial \Omega}{\partial \alpha_T^b} \tag{3.15a}$$

$$\dot{D}^d = [\frac{\partial^2 \Psi}{\partial D^d \partial D^d}]^{-1} \dot{\gamma}_D^d = [\frac{\partial^2 \Psi}{\partial D^d \partial D^d}]^{-1} \frac{\partial \Omega}{\partial D^d} \tag{3.15b}$$

which defines the evolution of the internal state. Eqs. (3.10) and (3.15) represent the flow and evolution laws, respectively. Both the state equations (3.4), (3.5), (3.6), and evolutionary laws must be satisfied for the general forms of GVIPS which has an assumed dissipation function $\Omega = \Omega(\sigma_{ij}, \alpha_T^b, D^d)$ and Gibb's potential wherein both potentials are directly linked through the internal state variables α_T^b and D^d (see eq. 3.15).

From eq. (3.15), the compliance operators are defined as follows:

$$L_{\alpha_T^b} = -\frac{\partial^2 \Psi}{\partial \alpha_T^b \partial \alpha_T^b} \quad ; \quad L_{D^d} = -\frac{\partial^2 \Psi}{\partial D^d \partial D^d} \tag{3.16}$$

they relate the "force-like" state variables ($\dot{\alpha}_T^b, \dot{D}^d$) to the "displacement-like" variables, provide a link between the assumed Gibb's and complementary dissipation potential, and ensures a number of desirable numerical features such as the symmetry of the resulting consistent tangent stiffness matrix. The above discussion provides the general thermodynamic framework in which the flow and evolution laws are associative.

3.3 Specific Form for GVIPS Model

Next, we use a specified form to constitute a GVIPS model. The emphasis is placed here on a careful examination of the mathematical structure of these governing equations. The transversely-isotropic viscoplastic material, together with the counterpart anisotropic

elastic-response component, for a solid reinforced by a single family of fibers as in [71-72], is assumed. The development and application of fairly comprehensive models for anisotropic materials may be referred to [1, 6, 9-10, 21, 47, 53, 55-56, 60-62, 73].

3.3.1 Elastic Response

The general viscoplastic models consist of an elastic response and a viscoplastic response. The hyperelastic response is assumed to be *linear*; i.e., a *quadratic* strain-energy-density function, U^e, is assumed to exist such that the Cauchy (true) stress components σ are given by

$$\sigma_{ij} = \frac{\partial U^e}{\partial \varepsilon^e_{ij}} = C^e_{ijkl}\varepsilon^e_{kl} \tag{3.17}$$

where a superscript "e" signifies an elastic component; and

$$\varepsilon_{ij} = \varepsilon^e_{ij} + \varepsilon^p_{ij} \tag{3.18}$$

in accordance with the basic hypothesis of the additive decomposition of total strain tensor, ε_{ij}, into its elastic, ε^e_{ij}, and inelastic strain components, ε^p_{ij}. In the above, C^e_{ijkl} denotes the *fourth-order, symmetric*, elastic moduli tensor; i.e. $C^e_{ijkl} = C^e_{klij}$.

3.3.2 The Viscoplastic Response

Now, specify that T=2, n_b=1, n_d=0, so only one second-order internal variable, which is the back stress (internal), is specified. An outline of the basic equations is therefore given here. The starting point is a postulate for the existence of a plastic potential function, Ω, in terms of

the invariants of the stress tensor, σ, the internal variable (kinematic-hardening or back stress tensor), α, such that

$$\Omega = \Omega\left(\sigma_{ij}, \alpha_{ij}, V_{ij}\right) = \Omega_1\left(\sigma_{ij}, \alpha_{ij}, V_{ij}\right) + \Omega_2\left(\alpha_{ij}, V_{ij}\right) \tag{3.19a}$$

$$\Omega = \Omega_1(F) + \Omega_2(G) \tag{3.19b}$$

$$\dot{\varepsilon}_{ij}^{p} = \frac{\partial \Omega}{\partial \sigma_{ij}} \tag{3.20a}$$

$$\dot{\gamma}_{ij} = -\frac{\partial \Omega}{\partial \alpha_{ij}} \tag{3.20b}$$

where the parentheses are used to indicate functional dependence on the arguments inside (·); and the overdot signifies a rate or time derivative.

The F and G are *quadratic* functions in terms of the invariants of the *deviatoric* components of the *effective* stress, (σ_{ij}-α_{ij}), and the back stress, α_{ij}, tensors, respectively.

$$F = \frac{1}{2}\left(\sigma_{ij} - \alpha_{ij}\right) M_{ijkl} \left(\sigma_{kl} - \alpha_{kl}\right) / K_t^2 - 1 \tag{3.21a}$$

$$G = \frac{1}{2}\left(\alpha_{ij}\right) M_{ijkl} \left(\alpha_{kl}\right) / K_t^2 \tag{3.21b}$$

in which the *symmetric* fourth-order tensor M_{ijkl} is a function of fiber orientation tensor V_{ij} (material-directionality) and is defined as:

$$M_{ijkl} = P_{ijkl} - \xi Q_{ijkl} - \frac{1}{2}\zeta R_{ijkl} \tag{3.22}$$

where

$$\xi = \frac{\eta^2 - 1}{\eta^2} \quad ; \quad \zeta = \frac{4(\omega^2 - 1)}{4\omega^2 - 1} \tag{3.23a}$$

$$\eta = K_l/K_t \quad ; \quad \omega = Y_l/Y_t \tag{3.23b}$$

and P_{ijkl}, Q_{ijkl} and R_{ijkl} are defined as follows:

$$P_{ijkl} = I_{ijkl} - \frac{1}{3}\delta_{ij}\delta_{kl} \quad ; \quad I_{ijkl} = \frac{1}{2}\left(\delta_{ik}\delta_{jl} + \delta_{il}\delta_{jk}\right) \tag{3.24a}$$

$$Q_{ijkl} = \frac{1}{2}\left(V_{ik}\delta_{jl} + V_{il}\delta_{jk} + V_{jk}\delta_{il} + V_{jl}\delta_{ik}\right) - 2V_{ij}V_{kl} \tag{3.24b}$$

$$R_{ijkl} = 3V_{ij}V_{kl} - \left(V_{ij}\delta_{kl} + V_{kl}\delta_{ij}\right) + \frac{1}{3}\delta_{ij}\delta_{kl} \tag{3.24c}$$

$$V_{ij} = v_i v_j \tag{3.24d}$$

where v_i is the unit vector defining the material fibre direction.

In the above, $0 \le \xi \le 1$ and $0 \le \zeta \le 1$ are material-strength ratios, and the constants K_t (or K_l) and Y_t (or Y_l) are threshold strengths of the composite material in transverse (or longitudinal) shear and tension/compression, respectively. For the isotropic case, $\xi = \zeta = 0$ and M_{ijkl} reduces to P_{ijkl}, i.e., simply the classical von Mises-type forms in functions F and G.

Because of n_b=1, n_d=0, for the present purely mechanical theory, Eq.(3.1) comes to the following *decoupled* form of a (Gibbs) *complementary* free-energy density function in terms of stress and internal state parameters [e.g. 39]; i.e., with superscripts "e" and "i" indicating elastic and inelastic parts,

$$\psi\left(\sigma_{ij}, \alpha_{ij}\right) = \psi^e\left(\sigma_{ij}\right) + \psi^i\left(\alpha_{ij}\right) \tag{3.25a}$$

we define ψ^e and ψ^I by the following forms:

$$\psi^e(\sigma_{ij}) = \frac{1}{2}\sigma_{ij} C^{e\ -1}_{ijkl}\sigma_{kl} \quad ; \quad \psi^i(\alpha_{ij}) = \frac{K_t^2}{(1+\beta)H} G^{1+\beta} \tag{3.25b}$$

and the (positive) material constants: H and K_t (stress units), and β (dimensionless), as well as function $G = G(\alpha_{ij})$ were defined previously in Eqs. (3.21b). Together with the strain vector decomposition of Eq. (3.18), the above Eqs. (3.25) define the *equations of state*:

$$\varepsilon_{ij} - \varepsilon^p_{ij} = \frac{\partial \psi^e}{\partial \sigma_{ij}} = C^{e\ -1}_{ijkl}\sigma_{kl} \quad ; \quad \gamma_{ij} = \frac{\partial \psi^i}{\partial \alpha_{ij}} = \frac{1}{h}\pi_{ij} \tag{3.26a}$$

$$h = H/G^{\beta} \quad ; \quad \pi_{ij} = M_{ijkl}\,\alpha_{kl} \tag{3.26b}$$

the dissipation function $\Omega\,(\sigma_{ij},\alpha_{ij})$ is now introduced naturally as follows:

$$\Omega = \sigma_{ij}\ \dot{\varepsilon}_{ij} - \dot{\psi} \geq o \tag{3.27a}$$

or, substituting for $\dot{\psi}$ in terms of $\dot{\sigma}_{ij}$ and $\dot{\alpha}_{ij}$ from (3.25a), one gets from (3.27a)

$$\frac{\partial \Omega}{\partial \sigma_{ij}} = \dot{\varepsilon}^p_{ij} \quad ; \quad \frac{\partial \Omega}{\partial \alpha_{ij}} = -\dot{\gamma}_{ij} \quad = \quad -\left(\frac{\partial^2 \psi^i}{\partial \alpha_{ij}\partial \alpha_{kl}}\right)\dot{\alpha}_{kl} \tag{3.27b}$$

The *rate* form presently connecting $\dot{\alpha}_{ij}$ and $\dot{\gamma}_{ij}$ through the Hessian matrix of ψ^i (hardening-moduli tensor) ,the time derivatives of the second of Eqs. (3.27), yields

$$\dot{\alpha}_{ij} = h\left[Z^m_{ijkl} + \frac{h'}{h(1+2\beta)}\alpha_{ij}\alpha_{kl}\right]\dot{\gamma}_{kl} = \left[L_{ijkl}\right]^{-1}\dot{\gamma}_{kl} \tag{3.28a}$$

where L_{ijkl} is called compliance operator, and h' is a scaled derivative,

$$h' = \frac{1}{k_t^2}\frac{dh}{dG} \tag{3.28b}$$

and we defined $Z^{m}_{ijkl} = M^{-1}_{ijkl}$ for the "generalized inverse" of $\underset{\sim}{M}$; see details for different conditions (three-dimentional, plane-strain/axisymmetric, generalized plane stress, etc) in Part II [38]. Now, the present model exhibits a potential structure, i.e., the elastic part is formulated in terms of a strain-energy density function, whereas a dissipation potential is utilized in the flow law for the inelastic strain rate and the nonlinear kinematic hardening-recovery type evolution equation for the internal state variable.

3.3.3 The Viscoplastic Response: Flow and Evolution Laws

From Eqs. (3.19-3.21) and (3.25-3.28), the final expressions for the inelastic flow and evolution equations are given as follows, for the specific selection of power functional forms for $\Omega_1(F)$ and $\Omega_2(G)$:

$$\dot{\varepsilon}^{p}_{ij} = f(F)\Gamma_{ij} \quad ; \quad \Gamma_{ij} = M_{ijkl}\,(\sigma_{kl}-\alpha_{kl}) \tag{3.29a}$$

$$\dot{\gamma}_{ij} = \dot{\varepsilon}^{p}_{ij} - \frac{\gamma}{h}\pi_{ij} \quad ; \quad \pi_{ij} = M_{ijkl}\alpha_{kl} \tag{3.29b}$$

$$\dot{\alpha}_{ij} = \left[L_{ijkl}\right]^{-1}\left(\dot{\varepsilon}^{p}_{ij} - \frac{\gamma}{h}\pi_{ij}\right) \tag{3.29c}$$

where f, h, and γ are the flow, hardening, and recovery functions, respectively. The latter are given in terms of their respective arguments as follows:

$$f(F) = F^{n}\Big/\left(2\mu K_t\sqrt{F+1}\right) \tag{3.30a}$$

$$h = H/G^{\beta} \quad ; \quad \gamma = R\,G^{m-\beta}\Big/\left(K_t\sqrt{G}\right) \tag{3.30b}$$

in which $n \geq 1$, μ, H, β, R, and $m \geq \beta + 1/2$ are (positive) material constants, and K_t was used previously in Eqs. (3.21) to (3.25).

Several regions of *discontinuities* in the state (σ_{ij}, α_{ij}) space were introduced to account for stress-reversal/cyclic-loading/dynamic-recovery effects. This simply amounts to using different functional forms for f, h, and γ in different regions; i.e.,

$$f = f \quad \text{if} \quad F > 0 \tag{3.31a}$$

$$f = 0 \quad \text{otherwise} \tag{3.31b}$$

$$G = G \quad \text{if} \quad G > G_0 \quad \text{and} \quad \text{dev}\left(\sigma_{ij} - \alpha_{ij}\right)\pi_{ij} > 0 \tag{3.32a}$$

$$G = G_o \quad \textit{otherwise} \tag{3.32b}$$

where the "small" constant (cut-off value) G_o is an "adjusted" parameter selected to fit the experimental data, and so as to prevent singularity in h when $G \to 0$, and dev( ) is the deviatoric part of ( ). Note that eqs. (3.22) provide the simplest form of internal loading-unloading criterion; i.e., with the evolution for the internal strain variables, $\dot{\gamma}_{ij}$, during loading according to eq. (3.29b), but with a different dissipation function during unloading giving a "magnified" rate of evolution, $\dot{\gamma}^{u}_{ij} = \left[L_{ijkl}\right]\left[L^{u}_{klmn}\right]^{-1}\dot{\gamma}^{l}_{mn}$, to account for the "stiffer" response upon unloading, with the moduli L^{u}_{ijkl} taken in the same form as for loading L_{ijkl} in eq. (3.28a) with G_0 replacing G. However, altenative criterion are also possible to handle these observed readjustment of internal state [4], and may actually have direct impact on such cyclic-loading phenomena such as ratchetting.

3.4 Generalized Viscoplasticity for Nonassociative Material

As discussed in section 3.1, the nonassociative models are those which possess a partially (i.e., using only the Ω-forms) or totally incomplete potential formulation. They either violate equations of state or evolution equations. Their popularity in the literature is mainly due to the added modeling flexibility to account for experimental phenomena by

using arbitrary rate forms in the flow and evolution equations. In this section, Freed's viscoplastic model [24] is used as an example to discuss the theoretical basis of the nonassociative models.

This viscoplastic model with creep and plasticity bounds was developed to represent the behavior of polycrystalline metals at high temperature, and is capable of accurately predicting short-term plastic strains, long-term creep strains and the interactions between them. It reduces analytically to a creep theory under steady-state conditions and becomes a plasticity theory at its rate-independent bound. This model is characterized by steady-state creep data, saturated hysteresis loops, and monatomic stress/strain curves. A general mathematical structure for viscoplasticity admits two tensorial internal variables, which are a short (α_{ij}^{s}) and a long (α_{ij}^{l}) back stress, and one scalar internal variable D, which is drag stress. In this model, the flow and evolution equations are no longer derived from Ω-forms. Due to the nonassociative behavior of this model, it will be verified that the consistent viscoplastic-moduli matrix is no longer symmetric when the implementation of this model is discussed in Part II of this report.

As mentioned, the discussion is limited to the case of an isotropic material under isothermal conditions. Freed's original model is temperature dependent, and some material constants are temperature dependent. Under the present isothermal conditions, temperature effect is canceled from the original model equations, and those material constants which are the function of temperature are fixed during calculation at a given temperature. Tests may be given at different temperatures as long as the given temperature does not change during a test. In order to utilize the general framework of the algorithm represented in the previous section, the original tensor equations [78], which have the plasticity bound and influence of temperature variation are restricted and recast into the format used in the algorithm of GVIPS to facilitate the implementation of NAV. To be clear, the original equations of Freed's model will be transformed into the new matrix format. (further details on these specific forms are given in Part II).

3.4.1. Elastic Behavior

The stress, σ_{ij}, is taken to be related to the infinitesimal total strain, ε_{ij}, through the constitutive equations of an isotropic Hookean material, viz.

$$S_{ij} = 2\mu\left(E_{ij} - \varepsilon^{p}_{ij}\right) \quad where \quad \varepsilon^{p}_{kk} = 0 \tag{3.33a}$$

and

$$\sigma_{kk} = 3\kappa\varepsilon_{kk} \tag{3.33b}$$

which are characterized by the shear, μ, and bulk, κ, elastic moduli, and where

$$S_{ij} = \sigma_{ij} - \frac{1}{3}\sigma_{kk}\delta_{ij} \quad \text{and} \quad E_{ij} = \varepsilon_{ij} - \frac{1}{3}\varepsilon_{kk}\delta_{ij} \tag{3.33c}$$

denote the deviatoric stress and strain, respectively. Eq. (3.33a) characterizes the deviatoric stress response, while eq. (3.33b) characterizes the hydrostatic stress response.

Based on the previous framework of section 3.3, the above equations of the elastic behavior are recast as,

$$\sigma_{ij} = C^{e}_{ijkl}\varepsilon^{e}_{kl} \tag{3.34a}$$

$$\varepsilon_{ij} = \varepsilon^{e}_{ij} + \varepsilon^{p}_{ij} \tag{3.34b}$$

where $\sigma_{ij}, \varepsilon_{ij}$ are the same definition as before. The shear modules G and elastic modules E are defined as follows:

$$G = \mu_0 + \mu_1 T \tag{3.35a}$$

$$E = 2\,(1+\nu)\,G \tag{3.35b}$$

where T is temperature and ν is Poisson's ratio. μ_0 and μ_1 are material constants.

3.4.2. Viscoplastic Behavior

Plastic flow equation:

$$\dot{\varepsilon}_{ij}^{p} = \left\|\dot{\varepsilon}^{p}\right\| n_{ij} \quad ; \quad n_{ij} = \frac{1}{2}\frac{s_{ij} - \alpha_{ij}}{\left\|\mathbf{s} - \boldsymbol{\alpha}\right\|} \tag{3.36}$$

whose kinetics are governed by

$$\left\|\dot{\varepsilon}^{p}\right\| = \vartheta Z \qquad \text{if } \left\|\mathbf{s} - \boldsymbol{\alpha}\right\| < \mathrm{K} \tag{3.37}$$

with the Von Mises norm $\quad \left\|s - \alpha\right\| = \sqrt{\frac{1}{2}\left(s_{ij} - \alpha_{ij}\right)\left(s_{ij} - \alpha_{ij}\right)}$ (3.38)

and where K > 0 denotes the plastic yield stress.

The norms (or magnitudes) pertaining to the deviatoric tensors of this section are defined by

$$\left\|\mathrm{I}\right\| = \sqrt{2\mathrm{I}_{ij}\mathrm{I}_{ij}} \quad \text{and} \quad \left\|\Pi\right\| = \sqrt{\frac{1}{2}\Pi_{ij}\Pi_{ij}} \tag{3.39}$$

where I_{ij} is any deviatoric "strain-like" tensor, and Π_{ij} is any deviatoric "stress-like" tensor.

Associated material functions quantifying plastic strain rate are as follows:

$$\vartheta = \begin{cases} \exp\left[\dfrac{-Q}{KT}\right] & \text{when } T_t \le T < T_m \\ \exp\left[\dfrac{-Q}{KT_t}\left(\ln\left[\dfrac{T_t}{T}\right] + 1\right)\right] & \text{when } 0 < T \le T_t \end{cases} \tag{3.40}$$

$$Z = A\sinh^{n}\left[\frac{\|s-\alpha\|}{D}\right] \tag{3.41}$$

Eq. 3.36 may be recast as follows:

$$\dot{\varepsilon}^{p}_{ij} = f(J,D)\Gamma_{ij} \quad ; \quad \Gamma_{ij} = M_{ijkl}(\sigma_{kl} - \alpha_{kl}) \tag{3.42}$$

where, f is the function of J and drag stress D, which is:

$$f = \vartheta A\frac{1}{2\sqrt{J}}Sinh^{n}\left(\frac{\sqrt{J}}{D}\right) \tag{3.43}$$

where J is quadratic function in terms of the invariants of the deviatoric components of the effective stress, $(\sigma_{ij} - \alpha_{ij})$. i.e.,

$$J = \|s_{ij} - \alpha_{ij}\|^{2} = \frac{1}{2}(\sigma_{ij} - \alpha_{ij})M_{ijkl}(\sigma_{kl} - \alpha_{kl}) \tag{3.44}$$

in which M_{ijkl} is defined in eq.(3.22). Due to the isotropic behavior assumed in the Freed's original model, $\xi = \zeta = 0$, and M_{ijkl} reduces to P_{ijkl} as defined in eq.(3.24a). All presently-used forms of this latter model are restricted to isotropic behavior; this is also the case here for all the tests performed later in section 4.

The (deviatoric, tensor-valued) back stress, α, accounts for kinematic (flow-induced, anisotropic) hardening effects. Here α is taken to be a finite sum of the individual back stresses, i.e., $\alpha_{ij} = \alpha^{s}_{ij} + \alpha^{l}_{ij}$, where α^{s}_{ij} is called the short-range back stress, and α^{l}_{ij} is called the long-range back stress [24]. The evolution of these back stresses is described through the deviatoric constitutive equations as follows:

Evolution equation:

$$\dot{\alpha}^{s}_{ij} = 2H_s\left(\dot{\varepsilon}^{p}_{ij} - \frac{\alpha^{s}_{ij}}{2L_s}\left\|\dot{\varepsilon}^{p}\right\|\right) \tag{3.45a}$$

$$\dot{\alpha}^{l}_{ij} = 2H_l\left(\dot{\varepsilon}^{p}_{ij} - \frac{\alpha^{l}_{ij}}{2L_l}\left\|\dot{\varepsilon}^{p}\right\|\right) \tag{3.45b}$$

where H_s, H_l are the short and long term hardening moduli, and L_s, L_l are the thermal limiting states of the short and back stress, respectively,

$$H_s = \mu \quad \text{and} \quad L_s = f\frac{(C-D)(D-D_0)}{\delta C} \tag{3.46a}$$

$$H_l = \frac{\mu}{H_0} \quad \text{and} \quad L_l = (1\text{-}f)\frac{(C-D)(D-D_0)}{\delta C} \tag{3.46b}$$

In eqs. (3.45), the first terms represent hardening while the second terms represent a deviation from strain hardening-a phenomenon called recovery. The evolution of the back stress accounts for the rapid change in stiffness that is observed during the transition from elastic to plastic behavior.

Evolution equations (3.45a,b) for the back stress may be recast as follows:

$$\mathrm{dev}\left(\dot{\alpha}^{s}_{ij}\right) = 2H_s\dot{\varepsilon}^{p}_{ij} - g_s\pi^{s}_{ij} \quad ; \quad \pi^{s}_{ij} = M_{ijkl}\alpha^{s}_{kl} \tag{3.47a}$$

$$\mathrm{dev}\left(\dot{\alpha}^{l}_{ij}\right) = 2H_l\dot{\varepsilon}^{p}_{ij} - g_l\pi^{l}_{ij} \quad ; \quad \pi^{l}_{ij} = M_{ijkl}\alpha^{l}_{kl} \tag{3.47b}$$

where, g_s, g_l are defined as:

$$g_s = \frac{H_s}{2L_s}\vartheta A\mathrm{Sinh}^{n}\left(\frac{\sqrt{J}}{D}\right) \tag{3.48a}$$

$$g_1 = \frac{H_1}{2L_1}\vartheta A \mathrm{Sinh}^n\left(\frac{\sqrt{J}}{D}\right) \qquad (3.48b)$$

Another internal variable D, the drag strength, accounts for isotropic hardening effects. Because of its scalar nature, the strain hardening and dynamic recovery terms are combined into a single, nonlinear, hardening function, and the evolution of the drag strength is as follows:

$$\dot{D} = h\left(\left\|\dot{\varepsilon}^p\right\| - \vartheta\gamma\right) \quad ; \quad D_0 \le D \le D_{max} \qquad (3.49)$$

in which the first term of eq. (3.44) represents hardening, the second term recovery. The drag strength is bound by the interval $D_0 \le D \le D_{max}$.

The hardening modules and other material constants for the drag strength are given as follows.

$$h = h_D\left(\frac{(D-D_0)/\delta C}{\sinh[(D-D_0)/\delta C]}\right)^m \qquad (3.50)$$

$$\gamma = A\sinh^n\left[\frac{D-D_0}{\delta C}\right] \qquad (3.51)$$

$$D_{max} = \frac{1}{2}\left(C + D_0\right) \qquad (3.52)$$

$$h_D = \begin{cases} h_1 & when\ T_t \le T < T_m \\ h_0 - \dfrac{h_0 - h_1}{T_t}T & when\ 0 < T \le T_t \end{cases} \qquad (3.53)$$

This viscoplastic model is constrained such that creep is its lower (steady-state) bound, and plasticity is its upper (rate-independent) bound. When at steady state (i.e., $\dot{\alpha}$=0, $\dot{D}$=0), this model reduces analytically to Odqvist's creep theory, which greatly

simplifies the model and the process of its characterization. When below the plastic yield surface, i.e. $F < 0$, (where, $F = \|s-\alpha\| - K$ or whenever $\|s-\alpha\| < K$), this model is a viscoplastic formulation.

From the above equations it is noted that there are 13 material constants required to characterize this viscoplastic model:

T_m , the melting temperature; $T_t = T_m/2$.
Q , the activation energy for self-diffusion.
ϑ , the thermal function.
H_s , H_l are the hardening modules of the short, long-range back stress, respectively.
f , the partitioning of back stress between short and long-range contributions.
A, C, D_0, δ, h_0, $h_{1,}$, m, n are other material constants used in the above eqs.

3.5 The Implicit Integration Scheme

Based on the theory discussed in the previous sections, the general implicit integration scheme is presented in this section. The details of the implementation and algorithm are discussed in Part II [38]. As mentioned, the Euler scheme is presently used as the integrator, since it shows superior stability and convergence properties and has become the proven standard for the numerical integration of the viscoplastic rate equations. In this section, all equations and expressions are shown using a concise matrix notation for the integrated stress and internal stress fields. The contracted (Voigt) representations in vector forms for the components of the corresponding symmetric, second-order, tensor are utilized, with a slight abuse in notation to indicate the vector-matrix representations, that is, matrices are defined by under-curved symbols and vectors by underlined symbols.

3.5.1 General Form of Newton Iterative Scheme

Consider a typical time step $t_n \rightarrow t_{n+1}$, where the state variables at step n are known. Assume that Δt and $\Delta \varepsilon$ are given in the total strain field. The basic problem of evolution, then, is to update the state variables in a manner consistent with the governing equations; i.e., evolution equations and flow equations for the state variables.

Using the implicit backward-Euler scheme, the update formulas are based on the following equation

$$\underline{\Sigma}_{n+1} = \underline{\Sigma}_n + d\underline{\Sigma}_{n+1} \tag{3.54}$$

where $\underline{\Sigma}_n$ is state variables, and $d\underline{\Sigma}_{n+1}$ is the increment of the state variables. n is the step counter. For the GVIPS model,

$$\underline{\Sigma}_n = \begin{pmatrix} \underline{\sigma}_n \\ \underline{\alpha}_n \end{pmatrix} \tag{3.55a}$$

whereas for the NAV model,

$$\underline{\Sigma}_n = \begin{pmatrix} \underline{\sigma}_n \\ \underline{\alpha}_{s_n} \\ \underline{\alpha}_{l_n} \\ D \end{pmatrix} \tag{3.55b}$$

and the expression for the state variables increment is

$$d\underline{\Sigma}_{n+1} = \left(\underset{\sim}{K}_{\Sigma} \right)^{-1} \underline{R}_{n+1} \tag{3.56}$$

where $\underset{\sim}{K}_{\Sigma}$ is the iterative Jacobi matrix of state variables and $\underline{R}_{n+1}$ is the residual function of state variables. The specific forms of $\underset{\sim}{K}_{\Sigma}$ and $\underline{R}_{n+1}$ for the GVIPS and NAV models are defined in Part II.

To determine the updated values for the state variables, a local iterative solution is needed based on the eqs. (3.54, 3.56). For a typical iteration k -> k+1,

$$\underline{\Sigma}_{n+1}^{k+1} = \underline{\Sigma}_{n+1}^{k} + d\underline{\Sigma}_{n+1}^{k} \tag{3.57}$$

note that $d\underline{\Sigma}_{n+1}^{k}$ are evaluated based on the last updated states which means the iteration scheme is implicit. This equation represents the classical Newton-Raphson iteration scheme. It is well known that the basic Newton scheme is of "local" character; i.e., exhibiting excellent convergence properties (asymptotically quadratic rate) only when the starting trial solution is near the converged value, but for the trial solution which is far away from the converged value, it becomes very difficult to converge. Therefore, more robust numerical schemes are required for complex nonlinear problems.

3.5.2 Line Search Scheme

As mentioned, for highly-nonlinear problems, although the implicit scheme described above is unconditionally stable, its successful application still requires the use of an advanced numerical technique such as a line search method to produce an effective, robust solution algorithm. Its purpose is to guide the solution towards convergence, and is accomplied by searching for a scalar multiplier that adjusts the amount of the iterative increment vector to be updated within each iteration based on the optimization theory.

The line search method was utilized successfully in the global finite element solution of practical problems such as concrete cracking [20], and there is well-document evidence that the use of the line search is also essential for robust performance of global Newton's method in inviscid elastoplasticity [68]. At the global level, the concept of the line search algorithm pertains to minimizing the potential energy, that is, the work done by the residual force due to the iterative displacement. Here, and in this same spirit, the line

search method is firstly applied at the local (material point) level to drive the residual constitutive functions to be zero based on the optimization theory.

Considering the line search method, eq. (3.57) need to be modified. Thus, for a typical iteration k -> k+1, the iterative procedure with line search may be described by the following expression.

$$\underline{\Sigma}_{n+1}^{k+1} = \underline{\Sigma}_{n+1}^{k} + \eta d\underline{\Sigma}_{n+1}^{k} \tag{3.58}$$

where η is a scalar ($1 \geq \eta \geq 0$) which adjusts the step size to optimize the iterative solution. Here, the objective of the line search method is to minimize $\left| \underline{R}_{n+1}^{k} \bullet d\underline{\Sigma}_{n+1}^{k} \right|$ based on the optimization theory. Here, "•" indicates the dot product of two vectors. In eq. (3.58), $\underline{\mathbf{R}}$ is the "vector-valued" residual function of the state variables. For the GVIPS model, this is written symbolically as

$$\underline{\mathbf{R}}^{k} = \begin{pmatrix} \underline{R}_{\sigma}^{k} \\ \underline{R}_{\alpha}^{k} \end{pmatrix} \tag{3.59a}$$

and for the NAV model,

$$\underline{\mathbf{R}}^{k} = \begin{pmatrix} \underline{R}_{\sigma}^{k} \\ \underline{R}_{\alpha_s}^{k} \\ \underline{R}_{\alpha_l}^{k} \\ R_{D}^{k} \end{pmatrix} \tag{3.59b}$$

For unconstrained problems, the residual comes from the difference between the current iterative value and the previous converged value. The calculations for $d\underline{\Sigma}$ depend on the residual function and its derivatives at the previous step. The specific forms of $\underline{\mathbf{R}}$ for GVIPS and NAV are defined in Part II [38].

Now consider,

$$s(\eta) = \underline{R}(\eta) \bullet d\underline{\Sigma}^k \tag{3.60}$$

in which $\underline{\Sigma}^k$ and $\Delta\underline{\Sigma}^k$ are fixed, and $\underline{R}$ and s are functions of η. When $\eta = 0$,

$$s_0 = s(\eta=0) = \underline{R}(\eta=0) \bullet d\underline{\Sigma}^k = \underline{R}_0 \bullet d\underline{\Sigma}^k \tag{3.61}$$

$\underline{R}_0$ is the residual function of the state variables at the end of the previous iteration. According to optimization theory, the best (optimum) solution is $s(\eta) = 0$, but numerically, this is not realistically possible and it is also inefficient to try and achieve this objective. In practical problems, a 'slack' line search is used, with the aim of making the magnitude of $S(\eta)$ small in comparison with that of $S(\eta=0)$, i.e.

$$\left| \frac{s(\eta)}{s(\eta = 0)} \right| < \beta_{ls} \tag{3.62}$$

where β_{ls} is the 'line-search tolerance'. Based on past research experience, a suitable value for β_{ls} is of the order of 0.8 [20]. After the successful search for η is completed, eq. (3.58) keeps updating state variables until they satisfy the convergence condition. More details of the line search method are discussed in Part II [38].

The convergence criterion here for Cauchy stress is in the following form,

$$\frac{\left\| \underline{\sigma}_{n+1}^{k+1} - \underline{\sigma}_{n+1}^{k} \right\|}{\left\| \underline{\sigma}_{n+1}^{k+1} \right\| + 0.01K_t} < tol \tag{3.63}$$

where, $\|\bullet\|$ is the Euclidean norm of vectors, and tol is tolerance. Other internal variables also have similar convergence criterion.

4. Applications

Considering the theoretical basis presented in the previous sections, a number of numerical tests are selected to demonstrate the capabilities, as well as various aspects, of the implicit iterative algorithm; e.g., validation, accuracy, robustness and computational efficiency. For any numerical method, accuracy, efficiency and a balance between the two are always major concerns. Validation of the algorithm may be proven by convergence and accuracy, while efficiency may be shown by CPU time comparisons with an explicit method or the same implicit method but with a different step size, but whose solution has the same accuracy.

In this section, the performance of the implicit algorithm for both GVIPS and NAV is tested. For NAV, the new line search technique outlined earlier in section 3 is used to improve the efficiency and also guarantee the convergence. The details of the particular line search scheme utilized here in Part II of this report. The subincrementing technique is not used in the implementation of the NAV model. In the GVIPS model, there are regions of discontinuities in the state (σ_{ij}, α_{ij}) space to account for stress-reversal effects, and for time steps during which these regions of discontinuity are traversed, the line search technique is no longer as powerful, as compared to the implementation of the NAV model (note that the line search is strictly valid only if the same "unique" forms of the residual functions apply during the considered step). Consequently, a subincrementing scheme is still needed to refine the global step size sufficiently to capture the point of discontinuity. For all other steps which are in the continuous region, the line search method will be shown to play an important role in terms of efficiency and convergence.

For all test cases, the material parameters used in GVIPS model are associated with W/Kanthal (a unidirectional mmc model material), whereas the material parameters used in the NAV model are for copper. Material constants for both classes of viscoplastic models are given in Appendix 1. Consequently, no direct comparison between the GVIPS

and NAV models can be made as the different test cases are performed with these two materials.

The solution schemes developed above were implemented in conjunction with a 4-node shell mixed finite element, as described in [66, 79]. All numerical simulations reported herein were obtained using this element.

4.1. Validation Tests

Here, various tests are used to validate the implicit integration algorithm for both the NAV and GVIPS models. These tests include tension, cyclic, creep, and relaxation tests performed with different load steps. Additionally, a nonproportional multiaxial loading test was examined using the NAV and GVIPS model. Note that an explicit, one-step forward Euler integrator was used to obtain a converged reference solution for comparison with the implicit integrator. For all tests of GVIPS, the load is transverse to fibers. Among all tests, some tests are designed for assessing numerical performance of both models, and others are taken according to literature [36].

Note that in the following tables, GIT is the average global iteration number, SUB is the average subincrement number, and LIT is the average local iteration number. Also, note that all of the CPU times are normalized with respect to the smallest CPU time. Here, CPU is the total time of a complete finite element analysis. Note that there are 8 integration points for one homogeneous element. For the implementation method in the following tables, the implicit method denotes the backward Euler scheme, whereas the explicit method denotes the forward Euler. Finally, for convenience, all validation tests discussed subsequently are based on a finite element mesh consisting of a single element representing a material point.

4.1.1. Tension Tests

This monotonic hardening test is used to demonstrate the accuracy and efficiency of the proposed implicit integration algorithm. For both NAV and GVIPS, the uniaxial, strain-controlled tensile test as shown in Fig. 1 was simulated. Where, the maximum applied strain was 0.20, and the total strain rate was 7.6×10^{-6}/s and 3.0×10^{-5}/s for NAV and GVIPS respectively.

4.1.1 (a) NAV Isotropic Model

Table 1 shows the results for a number of different load steps. First, note that the explicit integration method failed to reach the maximum strain level. After 10,000 steps, the explicit solution reached a maximum of 5% strain. To try and reach the maximum strain level, it was necessary to keep refining the step size, but this was stopped when the number of load steps and the CPU time became prohibitively large. From figure 2, the results of three different load step sizes are shown. The maximum stresses are 148, 148.57 and 148.82 MPa for the 73, 20, and 10 load steps, respectively, and the differences are less than 1%, thus demonstrating the accuracy of the integration algorithm. It also may be concluded that the 73 step test is the converged solution by comparing its results with the explicit method in the region up to 5% strain. The agreement with the explicit reference solution is also validation of the implementation of the implicit algorithm. With regards to CPU time, it is found that the ratios of the explicit method, in the region up to 5% strain, and 73 step implicit method, in the region up to 5% strain, is 200/2.5=80, and the ratio of 73 and 10 step cases is 3.2, which demonstrates the efficiency of the scheme. As an aside, the fact that the explicit solution required 10,000 steps is characteristic of explicit methods in general. For example, recent work by Arya [7] required from 40,000 to 100,000 iterations.

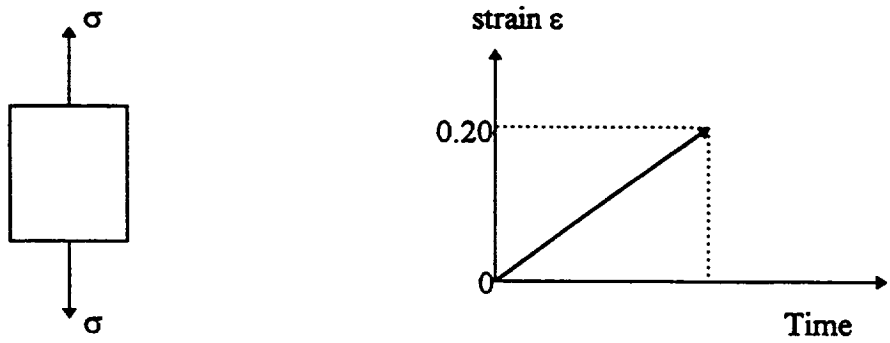

Figure 1 Tension Schematic

Table 1 Tension results for NAV

Copper , Temperature=121 C° , $\dot{\varepsilon}$=7.6 x 10^{-6}/s , ε_{max}=0.20 , $D_{t=0}$=0.57 Mpa

method	number of load steps	CPU time	GIT	LIT
explicit	10,000	> 200	1	0
implicit	73	3.2	2	7
implicit	20	1.1	3	8
implicit	10	1 (77 s)	3	9

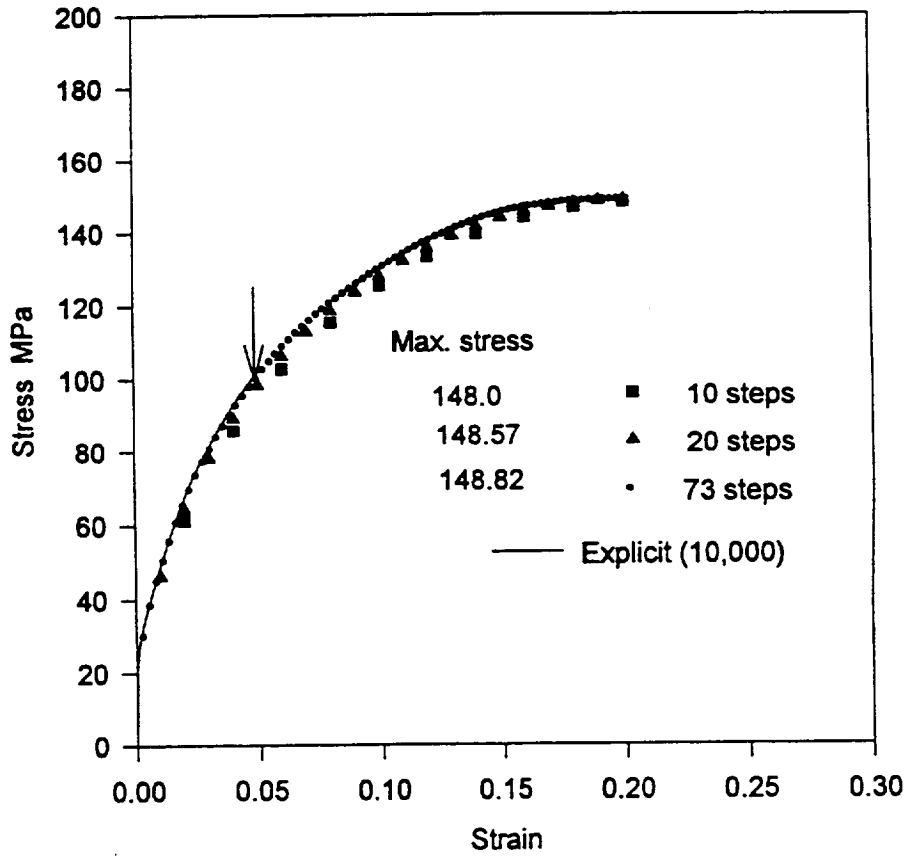

Figure 2 Tension results for NAV (121 C°)

4.1.1 (b) GVIPS Anisotropic Model

Table 2 illustrates the results for three different load step increments, utilizing the GVIPS model. Once again, 10,000 steps were applied for the explicit solution, here however, the explicit solution reached the maximum strain. The results of three different cases are the same as shown in fig. 3, thus demonstrating the accuracy of the integration algorithm and also the validation of the implementation of the implicit algorithm. The conclusion may be drawn that the 10 step case is the converged solution by comparing its results with the explicit method. With regards to CPU time, it is found that the ratios of the explicit method and the 10 step implicit method is 312, and the ratio of the 100 and 10 step case is 2.0, thus demonstrating the efficiency of the scheme.

4.1.2. Cyclic Loading Tests

This example serves to assess the accuracy of the stress predictions and to demonstrate the robustness of the implicit algorithm. For both NAV and GVIPS, the uniaxial, cyclic (non-monotonic), strain-controlled test, shown in Fig. 4, was simulated. The maximum strain amplitude was ±0.144 percent applied at a rate of 0.002/s.

4.1.2(a) NAV Isotropic Model

As shown in figure 5, the 100, 10, and 5 step cases agree reasonably with the converged explicit solution. For the 5 step case, the stress is updated from approximately -220 MPa to 200 MPa within one step, which demonstrates the robustness of the algorithm. Comparing the 100 step case with the explicit method which needs 10,000 global steps for one complete cycle, the CPU time ratio is approximately 340/6≅60 (table 3). Considering the comparable accuracy of these two cases, a CPU ratio of 60

Table 2 Tension results for GVIPS

W/Kanthal , $\dot{\varepsilon}=3.0 \times 10^{-5}/s$, $\varepsilon_{max}=0.20$

method	number of load steps	CPU time	GIT	LIT
explicit	10,000	312	1	0
implicit	100	2.0	2	3
implicit	10	1.0 (73 s)	3	4

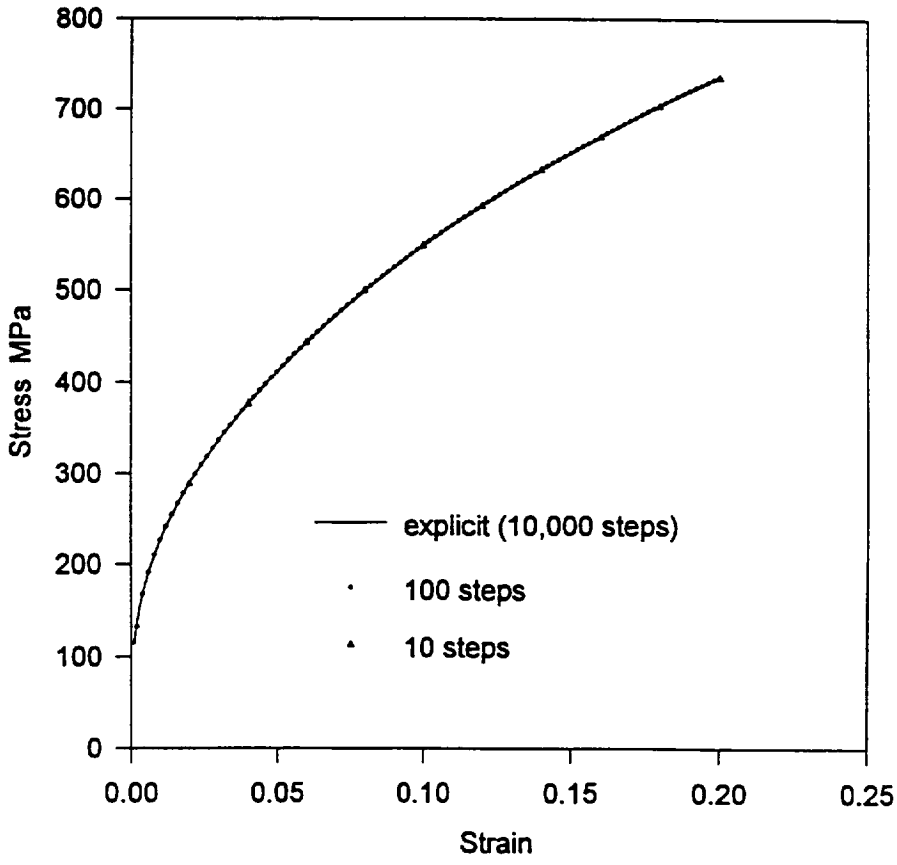

Figure 3 Tension results for GVIPS

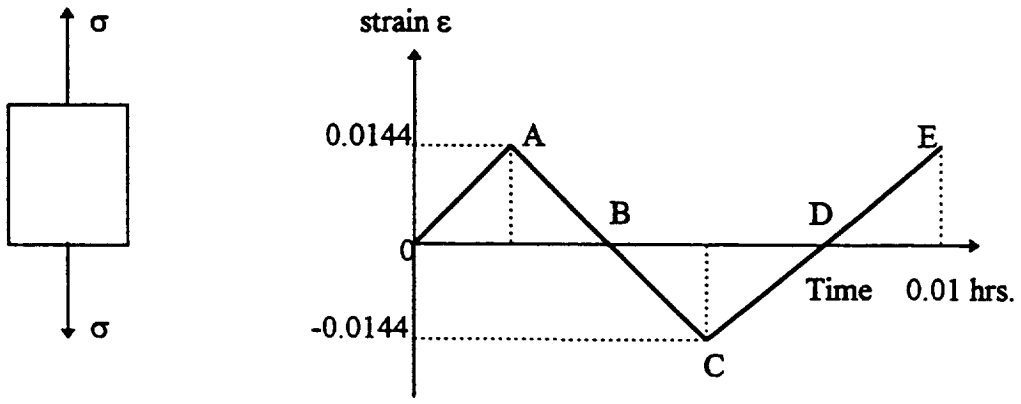

Figure 4 Cyclic Schematic

Table 3 Cyclic results for NAV

Copper , Temperature=21 C° , $\dot{\varepsilon}=2\times10^{-3}$/s , $\varepsilon_{max}=0.0144$, $D_{t=0}=5.9$ MPa

method	number of load steps	CPU time	GIT	LIT
explicit	10,000	340	3	0
implicit	100	6.0	2	4
implicit	10	1.05	3	10
implicit	5	1 (38 s)	3	22

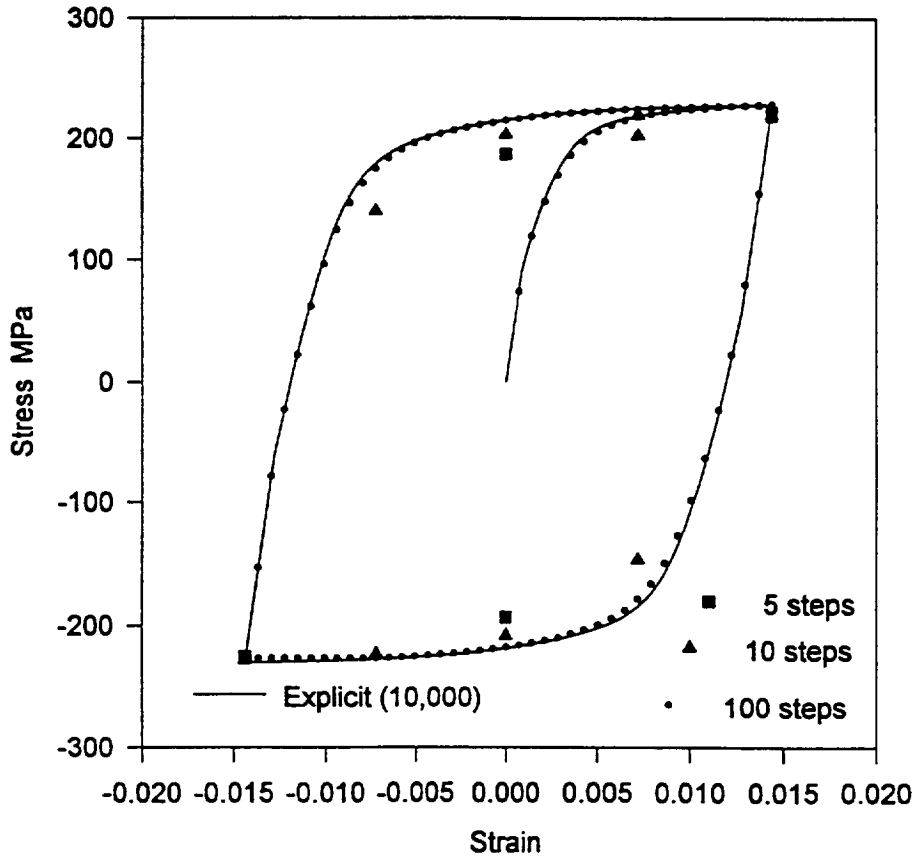

Figure 5 Cyclic results for NAV (21 C°)

demonstrates a significant improvement in efficiency and may be attributed to the use of the line search method.

4.1.2(b) GVIPS Anisotropic Model

Figure 6 shows the explicit converged solution as compared to the implicit 100, 10 and 5 step cases. The fact that all of the implicit cases match the converged solution demonstrates the accuracy, efficiency and robustness of the algorithm. In addition note that even the 5 step case matches the converged solution at all points of the hysteresis loop. The previously discussed discontinuities within the GVIPS formulation occurs along the path from A to B and from C to D as shown in figure 4. Those steps which contain the discontinuity point require subincrementing in order to cross the discontinuity. Taking the 10 step case as an example, the third and seventh global steps contain the discontinuity. Thus, only these two steps required subincrements which averaged 22 in this case. As such, comparing the 10 step case with the explicit solution (table 4), the CPU ratio is approximately 180 which demonstrates a marked saving in CPU time yet with comparable accuracy.

4.1.3. Creep Tests

The creep test is used to test both the accuracy and robustness (stability) of the implicit integration algorithm. In a creep test, the primary creep region is controlled by accuracy due to the high inelastic strain rates involved. In the secondary (steady state) creep region, the stability or robustness of the integration algorithm is tested. Both the NAV and GVIPS models will be used in the creep tests. For the NAV model one creep test of 1000 seconds will be performed, at a constant creep stress of 24 Mpa, whereas for the GVIPS model, one creep test of 1800 seconds at a creep stress of 70 MPa will be performed. Note in Fig. 7, ε_0 is the total strain at the beginning of the hold time and ε_f is

Table 4 Cyclic results for GVIPS

W/Kanthal , $\dot{\varepsilon}=2\text{x}10^{-3}$/s , $\varepsilon_{max}=0.0144$

method	number of load steps	CPU time	GIT	LIT
explicit	10,000	180.0	3	0
implicit	100	5.0	2	4
implicit	10	1.05	4	10
implicit	5	1 (54 s)	10	20

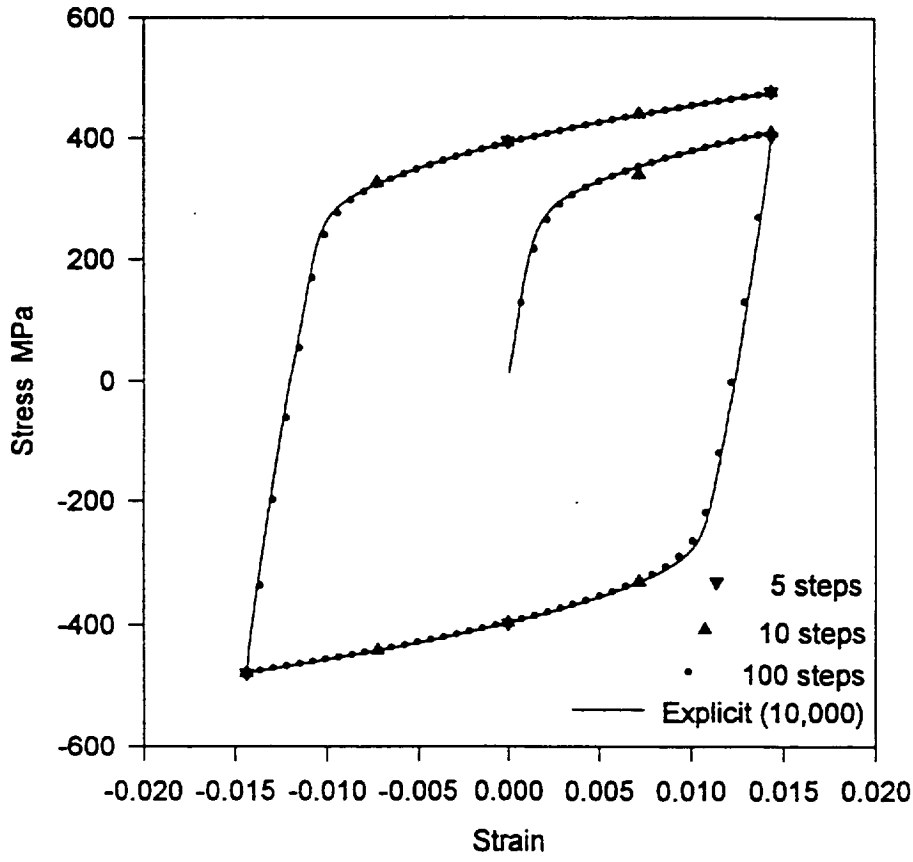

Figure 6 Cyclic results for GVIPS

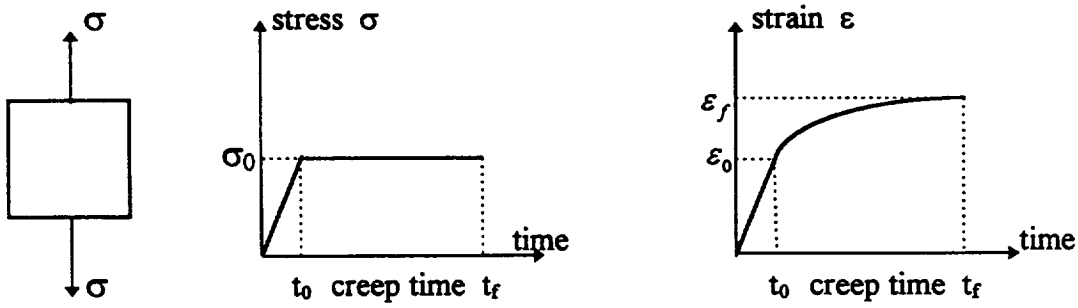

Figure 7 Creep Schematic

the amount of total strain at the end of the hold time. A large initial loading rate was chosen for both creep tests such that the initial load-up region may be considered as a purely elastic loading without any inelastic strain.

4.1.3(a) NAV Isotropic Model

The explicit method with a total of 20,400 global steps was determine to have converged and is used as the reference solution (Fig. 8). The implicit method, was run using 480 and 880 steps (table 5). With the 880 step case producing a solution that differs from the converged solution by approximately 1%. Note that it is in the primary creep region where accuracy is most important. It is well established that a larger number of steps are required to satisfy the requirement of high accuracy for the rate-dependent problem. With regards to CPU time, upon comparing the explicit method with the 880 step implicit case, there is a ratio of 32/1.6=20 which is a significant reduction in computation time.

4.1.3(b) GVIPS Anisotropic Model

The converged solution was obtained using the explicit method with a total of 5840 global steps (Fig. 9). Note that the difference between the explicit method and 805 step implicit method is less than 2% (table 6). Comparing CPU times, the ratio between the explicit method and the 805 step case is approximately 6.0, which demonstrates the efficiency of the implicit method. The 405 step case has a comparatively large error in comparison with the explicit solution. But, note that the secondary creep rate of the 405 step case does appear to match that of the converged solution. As expected, since the error may be attributed to the step size (accuracy and not stability), an improved primary creep response was predicted (805 step case) thus basically shifting the curve upward and closer to the converged solution.

Table 5 Creep results for NAV

Copper , Temperature=121 C° , σ_0=24 Mpa, $\dot{\sigma}$ = 2.4Mpa /s , $D_{t=0}$=0.57 MPa

method	number of load steps	CPU	ε_0 (10^{-3})	ε_f (10^{-3})	GIT	LIT	creep time (s.)
explicit	20,400	32	0.6273	0.8114	1	0	1000
implicit	880	1.6	0.6313	0.8022	2	1	1000
implicit	480	1 (954s)	0.6313	0.7853	3	2	1000

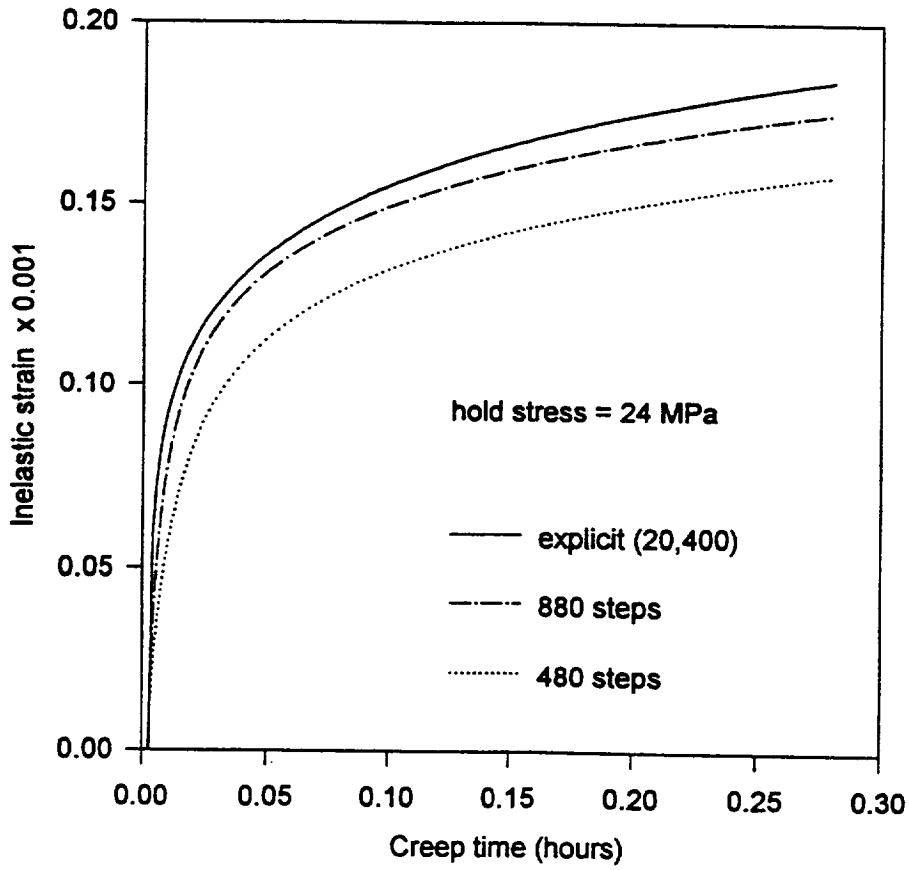

Figure 8 Creep results for NAV (121 C°)

Table 6 Results of creep tests for GVIPS

W/Kanthal , σ_0 = 10 ksi, $\dot{\sigma}$ = 1 ksi/s

method	number of load steps	CPU (s.)	ε_0 (10^{-3})	ε_f (10^{-3})	GIT	LIT	creep time (sec.)
implicit	405	1 (700)	0.3850	1.1016	2	2	1800
implicit	805	1.7	0.3850	1.2630	2	1	1800
explicit	5840	11.0	0.3759	1.2884	2	0	1800

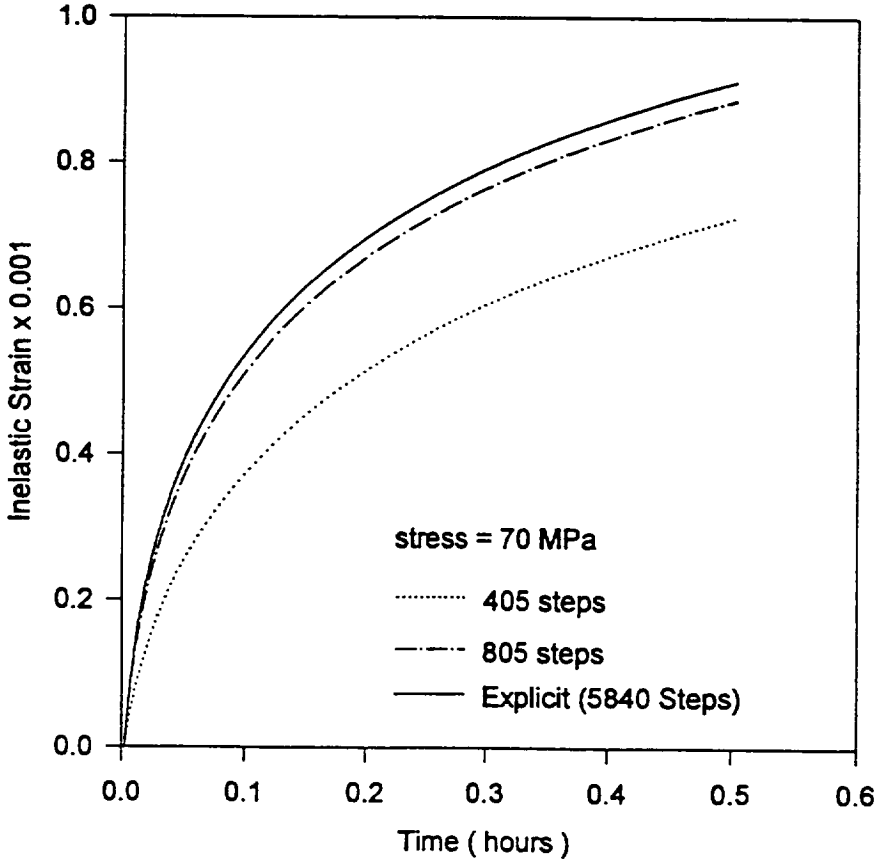

Figure 9 Creep results for GVIPS

4.1.4. Relaxation Tests

The stress relaxation test may also be used to assess the accuracy of the integration method. Subsequent to load up, typically, the relaxation test, Fig. 10 is characterized by a marked decrease in the initial stress at a high rate. The amount of stress relaxation and corresponding rate is dependent on the specific material model. Thus, an accurate integration method is required so as to properly predict the highly non-linear stress response. Relaxation tests were performed for both the NAV and GVIPS models. For the NAV model, the constant strain is 0.01 and the relaxation time for the test is 1000 seconds. Whereas for GVIPS, the constant strain is also 0.01, but the relaxation time is 1800 seconds.

4.1.4(a) NAV Isotropic Model

The converged, reference solution for the 1,000 second relaxation test using the explicit method required a total of 80,000 steps (table 7). This large number of steps was required to accurately predict the highly non-linear stress response. The implicit method was run using 110 and 210 steps, with the 210 step case essentially matching the converged solution (Fig. 11). Again, note that it is in the region where the stress decreases at a high rate that the solution is most sensitive to accuracy. Comparing the CPU time between the explicit and the 210 step implicit, there is a ratio of 900 in CPU time. Thus for comparable accuracy, the implicit method is far more efficient. As an aside, note that there is no significant predicted stress relaxation (i.e. < 4 MPa) for Freed's model. This may be due to the simplifying assumption that there is no explicit thermal recovery of the short- and long-range back stresses in his model.

4.1.4(b) GVIPS Anisotropic Model

The converged solution using the explicit method required a total of 3894 global steps (table 8). Fig. 12 shows the results for 22, 52 and 102 steps. Note that it is in the

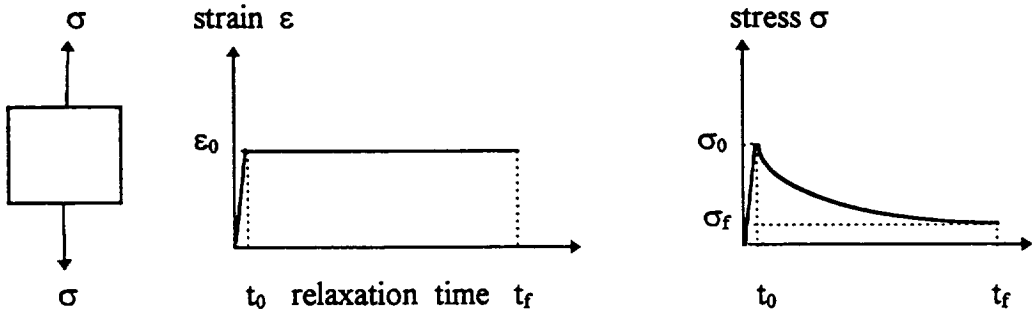

Figure 10 Relaxation Schematic

Table 7 Relaxation results for NAV

Copper , Temperature=316 C° , $\varepsilon_f = 0.01$, $\dot{\varepsilon}=1x10^{-3}$ s^{-1} , $D_{t=0}$=0.50 MPa

method	number of load steps	CPU	σ_0 MPa	σ_f MPa	GIT	LIT	relaxation time (s)
explicit	80,000	1350	36.331	32.848	1	0	1000
implicit	210	1.5	36.248	32.879	2	1	1000
implicit	110	1 (160s)	36.248	33.093	2	2	1000

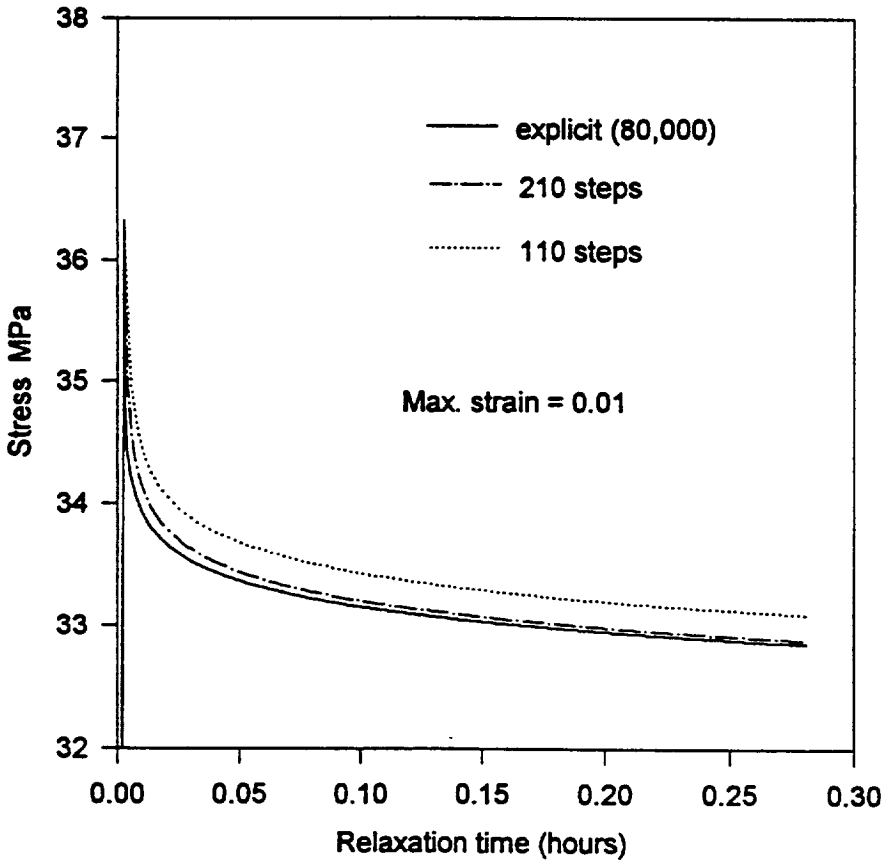

Figure 11 Relaxation results for NAV (316 C°)

Table 8 Results of relaxation tests for GVIPS

W/Kanthal , $\varepsilon_f = 0.01$, $\dot{\varepsilon}=1\text{x}10^{-3}\ s^{-1}$

method	number of load steps	CPU (s)	σ_0 ksi	σ_f ksi	GIT	LIT	relaxation time (s)
implicit	52	1 (71)	49.887	24.316	2	2	1800
implicit	102	1.8	49.887	23.625	2	1	1800
explicit	3894	53.9	50.701	23.430	2	0	1800

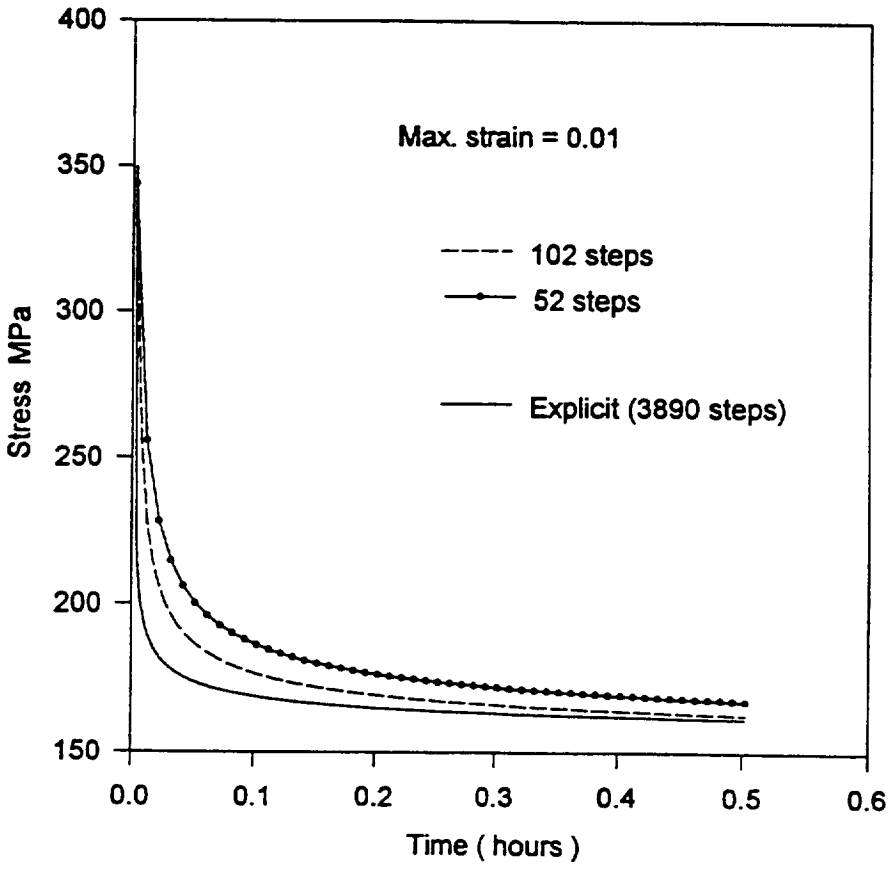

Figure 12 Relaxation results for GVIPS

initial relaxation region, (time < 0.2 hrs.) in which the solution is most sensitive to time step size and thus accuracy. The difference between the explicit method and the 102 step implicit case is less than 1% at the end of the relaxation period and approximately 8% difference at 0.05 hrs, where the solution is highly non-linear. Again, comparing the CPU time between the explicit and 102 step implicit methods, it is shown, see table 8, that a speed up ratio of approximate 30 times is indicated. Once again illustrating the efficiency of the implicit method. Finally, note that GVIPS predicts a significant amount of stress relaxation as suggested by experimental evidence, that is, approximately a 50% reduction in the initial stress after load up.

4.1.5 Nonproportional Multiaxial Tests

This final test examines the integration algorithm under nonproportional loading conditions. The element is subjected to the nonproportional strain path shown on Fig. 13. This path is taken from the experimental work of Lamba and Sidebottom [36]. This applied strain path was chosen because of its wide range of angles between segments with equal positive and negative peaks. The 8 paths combine shear, axial loading and unloading. The end points of the path segments were numbered from 0 to 8 and the path was traversed in a numerically increasing sequence. Note that the experiment given in Ref. [36] was conducted on a saturated specimen, that is, complete stabilization with regards to hardening has occurred.

4.1.5(a) NAV Isotropic Model

The stress response of the model to the applied nonproportional strain path appears in Fig. 14. This test demonstrates the robustness of the scheme discussed. The predicted response, shown in Figure 14, matches the experimental results (not shown in fig. 14) given in Ref. [36] very well. In addition, note that even one step per path (figure 14) can successfully complete this complicated loading history. Because the 50 step and 10 step cases give identical results, it is concluded that 50 steps has converged to the

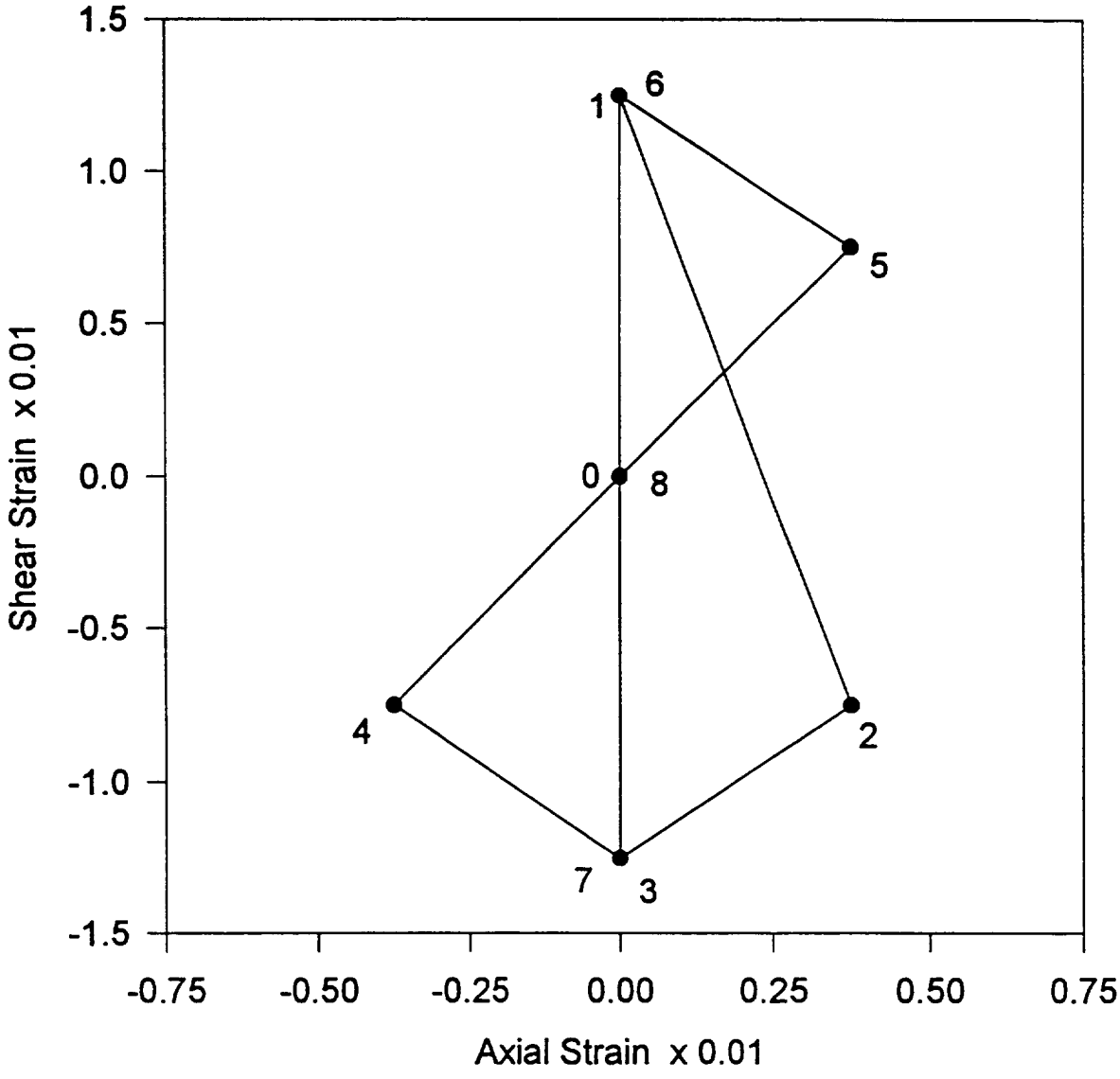

Figure 13 Nonproportional loading path

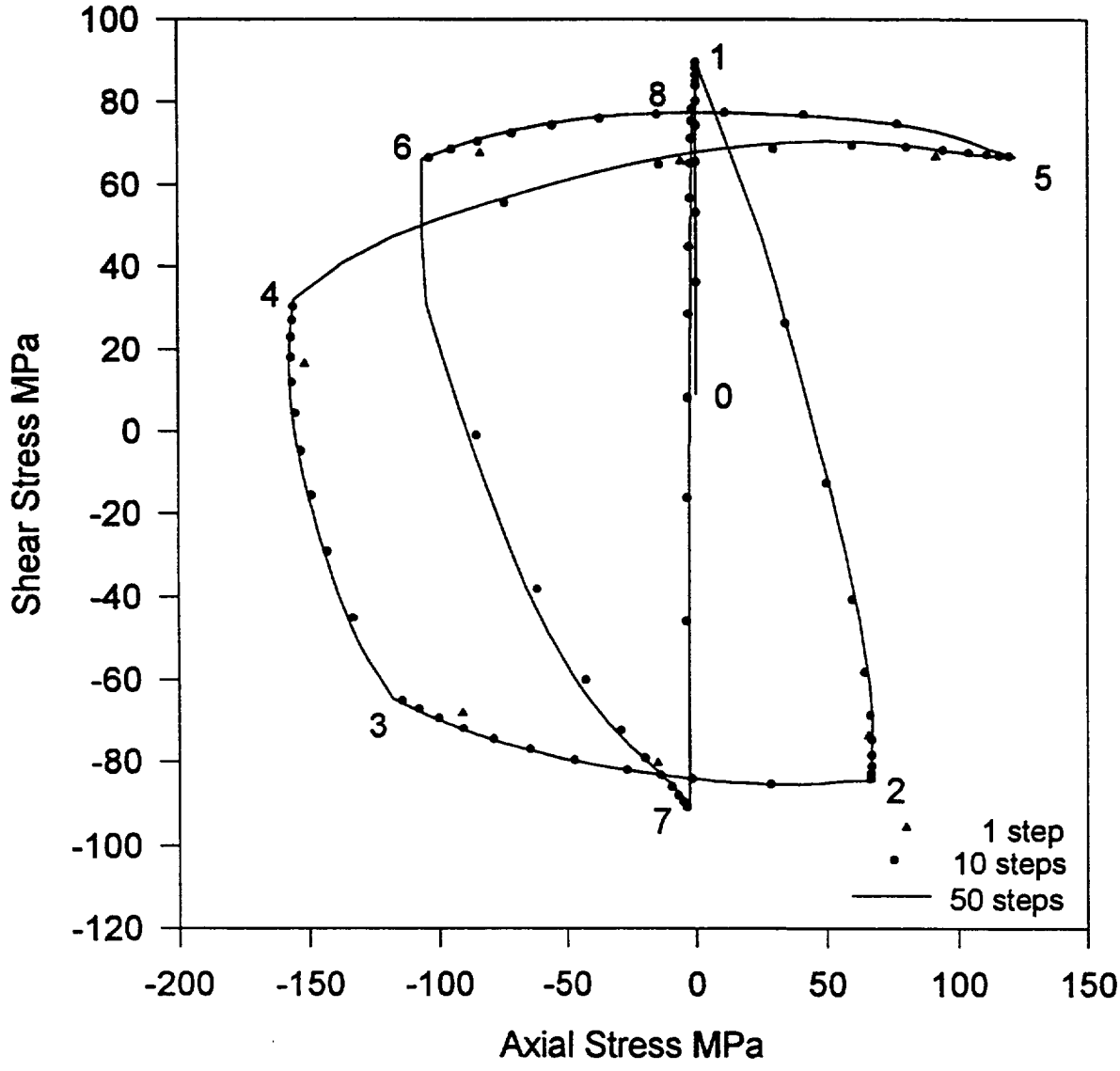

Figure 14 Nonproportional loading results for NAV (121 C°)

correct solution. Finally the CPU time for 1, 10, 50 steps per path are 1 (35s), 3.8 and 21.4, respectively.

4.1.5(b) GVIPS Isotropic Model

This GVIPS model was originally used to characterize W/Kanthal whose material constants are given in Appendix 1. In order to compare the stress response of the GVIPS model under nonproportional strain path with the experiment given in [36], the material constants needed to be changed to fit the copper material used in the experiment. The new material constants are given in Appendix 2, wherein the material is taken to be isotropic, i.e., $\omega=\eta=1.0$. Based on the new material constants, the predicted response of the GVIPS model is shown in Fig. 15, with the 10 step and 100 step cases giving almost identical results. Given the very crude characterization of the GVIPS model (essentially fitting the limit state in a single pure shear test), it is remarkable how accurate it represents the experimental results.

4.2. Efficiency : Comparative Studies

In addition to validating the proposed integration method, efficiency studies are necessary since efficiency is a very important feature that is required in order to solve large, realistic finite element problems. For such practical problems, it is desirable and necessary to obtain an accurate solution in the most economical manner, that is, using the minimum CPU time.

Many mathematical techniques have been applied in order to develop computationally efficient methodologies for nonlinear analyses in which a large global time step size may be chosen in order to reach convergence with sufficient accuracy. Subincrementing has been shown to be successful in guaranteeing convergence when using a large global time step. The basic idea in subincrementing is to refine the global step size to achieve local

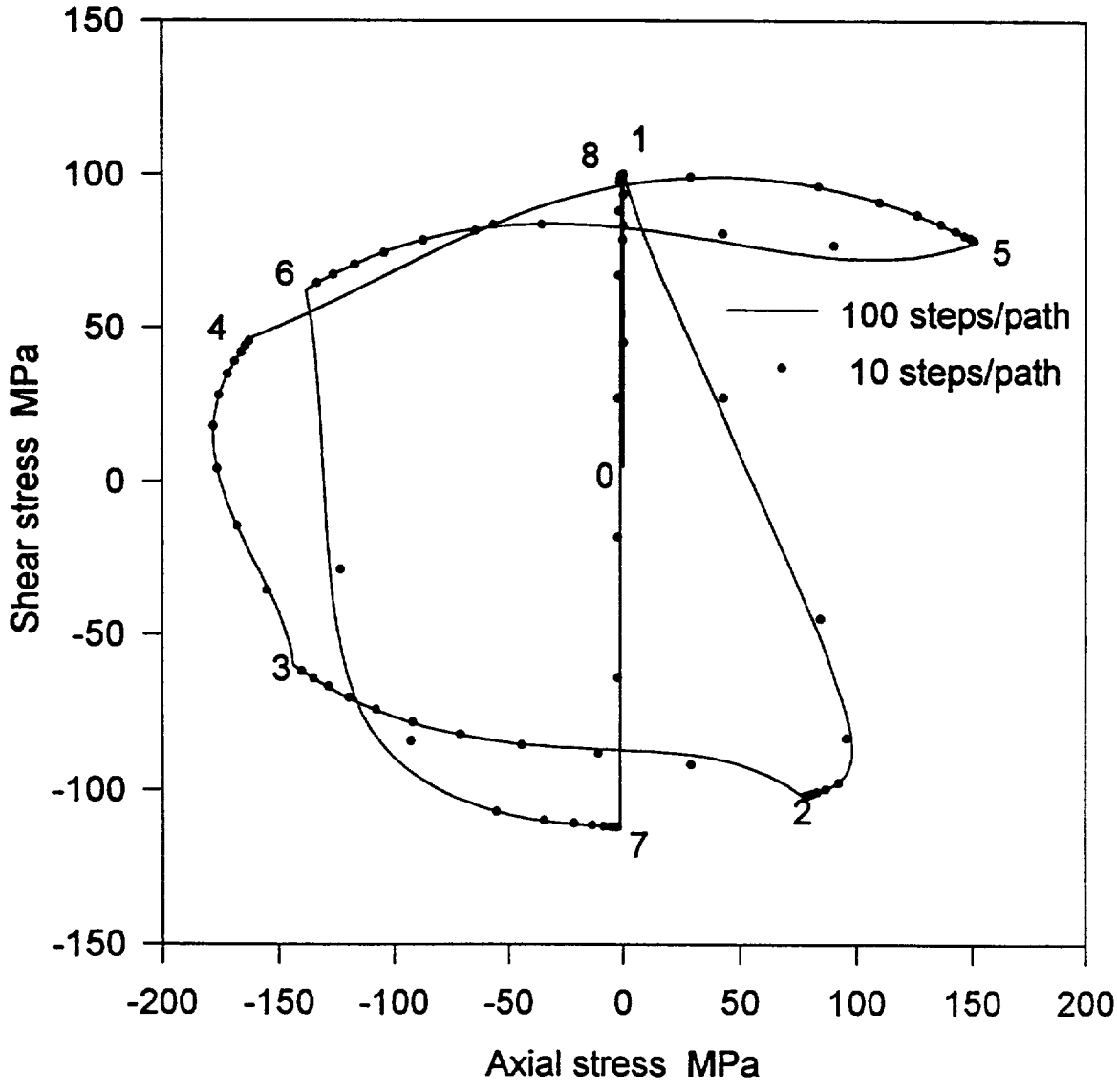

Figure 15 Nonproportional loading results for GVIPS

iteration convergence, as well as maintaining sufficient accuracy with regards to the updated fields, i.e. internal, state variables, stress, strain. For difficult load histories such as the cyclic test or for a complex, numerically stiff constitutive model, such as Freed's NAV, too many subincrements may be required, which directly results in large CPU times. Basically, subincrementing is useful for improved convergence, but it is not efficient since it does not improve the rate of convergence. Also, to date, there seems to be no agreement with regard to a single criterion of general applicability for determing the "optimal" number of subincrements. With these points in mind, a line search method was introduced here as a viable, and far more effective, alternative in providing improved convergence and solution economy. A detailed discussion of the line search method will be presented in Part II [38].

In order to compare the efficiency between the line search method and the subincrementing method, all the tests described below were performed using both of the two methods. In the following, Method 1 utilizes subincrementing only, while Method 2 utilizes only the line search method. Recall that for GVIPS, there are regions of discontinuities in the state space to account for stress-reversal effects which are loading and unloading conditions. In these steps, subincrementing is combined with line search in order to refine the step size to locate the point of discontinuity. This is required since the premise of line search is that equations optimized are continuous. Thus, Method 2 consists of a combination of subincrementing and line search methods, when the GVIPS model is utilized under cyclic loading conditions. For either the NAV or GVIPS model under monotonic loading condition, Method 2 is a line search only method. The results presented in tables 9 and 10 demonstrate the advantage of using a line search in the integration algorithm.

Comparing method 1 and 2 in the above tables, note that the CPU time of method 1 is always larger than the CPU time of method 2. In particular for GVIPS, the CPU ratios are 6.0, 4.5, 1.5, and 1.1 for the tension, cyclic, creep, and relaxation tests, respectively. For NAV, the CPU ratios are 13.65, 14.5, 1.55, and 22.2 for the tension, cyclic, creep,

Table 9 Results of comparision for GVIPS

Table 9a tension test. global steps=10 ϵ_{max}=0.20

Method	CPU (seconds)	GIT	SUB	LIT
subincrementing	6.0	11	11	3
line search *	1 (73)	3	0	4

Table 9b cyclic test. global steps=25 ϵ_{max}=0.0144

Method	CPU (seconds)	GIT	SUB	LIT
subincrementing	4.5	3	8	2
line search *	1 (33.91)	2	0	4

Table 9c creep test. global steps=105 σ=70 MPa

Method	CPU (seconds)	GIT	SUB	LIT
subincrementing	1.5	4	4	2
line search *	1 (178)	4	0	2

Table 9d relaxation test. global steps=105 ϵ_{max}=0.01

Method	CPU (seconds)	GIT	SUB	LIT
subincrementing	1.1	3	2	2
line search *	1 (122)	3	0	2

* Combination of the line search method and subincrementing (only when crossing regions of discontinuity).

Table 10 Results of comparision for NAV

Table 10a tension test. global steps=10 ϵ_{max}=0.20

Method	CPU (seconds)	GIT	SUB	LIT
subincrementing	13.65	16	15	3
line search	1 (77)	3	0	9

Table 10b cyclic test. global steps=5 ϵ_{max}=0.0144

Method	CPU (seconds)	GIT	SUB	LIT
subincrementing	14.5	8	15	5
line search	1 (38)	3	0	22

Table 10c creep test global steps=23 σ=70 Mpa

Method	CPU (seconds)	GIT	SUB	LIT
subincrementing	1.55	25	15	5
line search	1 (768)	20	0	15

Table 10d relaxation test. global steps=22 ϵ_{max}=0.01

Method	CPU (seconds)	GIT	SUB	LIT
subincrementing	22.2	6	24	2
line search	1 (50)	2	0	3

and relaxation tests, respectively. For NAV the largest CPU ratio is 22.2, i.e., method 2 with line search is approximately 95% faster than method 1 with subincrementing. This shows a significant improvement in efficiency particularly for a problem which requires accuracy, as in the case of the relaxation test. With regards to the number of iterations both globally and locally, line search usually required more local iterations, but this is due to the fact that it does not use any subincrements. From the results, it is apparent that the small additional local calculations required for the line search method leads to a saving in the total calculations. Specifically, some tests may need a large number of subincrements. For example, in the relaxation test of NAV, the number of subincrements for method 1 is 24 with 2 local iterations, table 10b. On the other hand, with line search, method 2, only 3 local iterations are required, thus resulting in a significant reduction in CPU time.

Finally, comparing tables 9, and 10, notice that for GVIPS, the CPU ratios of method 1 to method 2 are always less than NAV's. This trend may indicate that it is more difficult to integrate NAV without the help of sophisticated numerical techniques. On the other hand, since line search does not appear to significantly affect local convergence, GVIPS may be comparably easier to integrate and may only require a simple subincrementing scheme.

4.3. A General Structural Problem Using a NAV Isotropic Model

As has been stated throughout this report, the ultimate test of the integration method is to demonstrate its accuracy, robustness and efficiency when applied to a realistic structural analysis problem. In this context, a perforated plate as presented in reference [29] and [76], was analyzed using Freed's NAV model. A quarter of the plate is discretized for FE analysis (see figure 16). A linearly increasing specified displacement, with a maximum value of 0.5 percent ($\Delta l/w$) at a rate of 6.67×10^{-5}/s, was applied along the upper boundary of the plate. Material constants are the same as those given in Appendix 1. The results shown in Figure 17-19 are the effective stress distribution at the

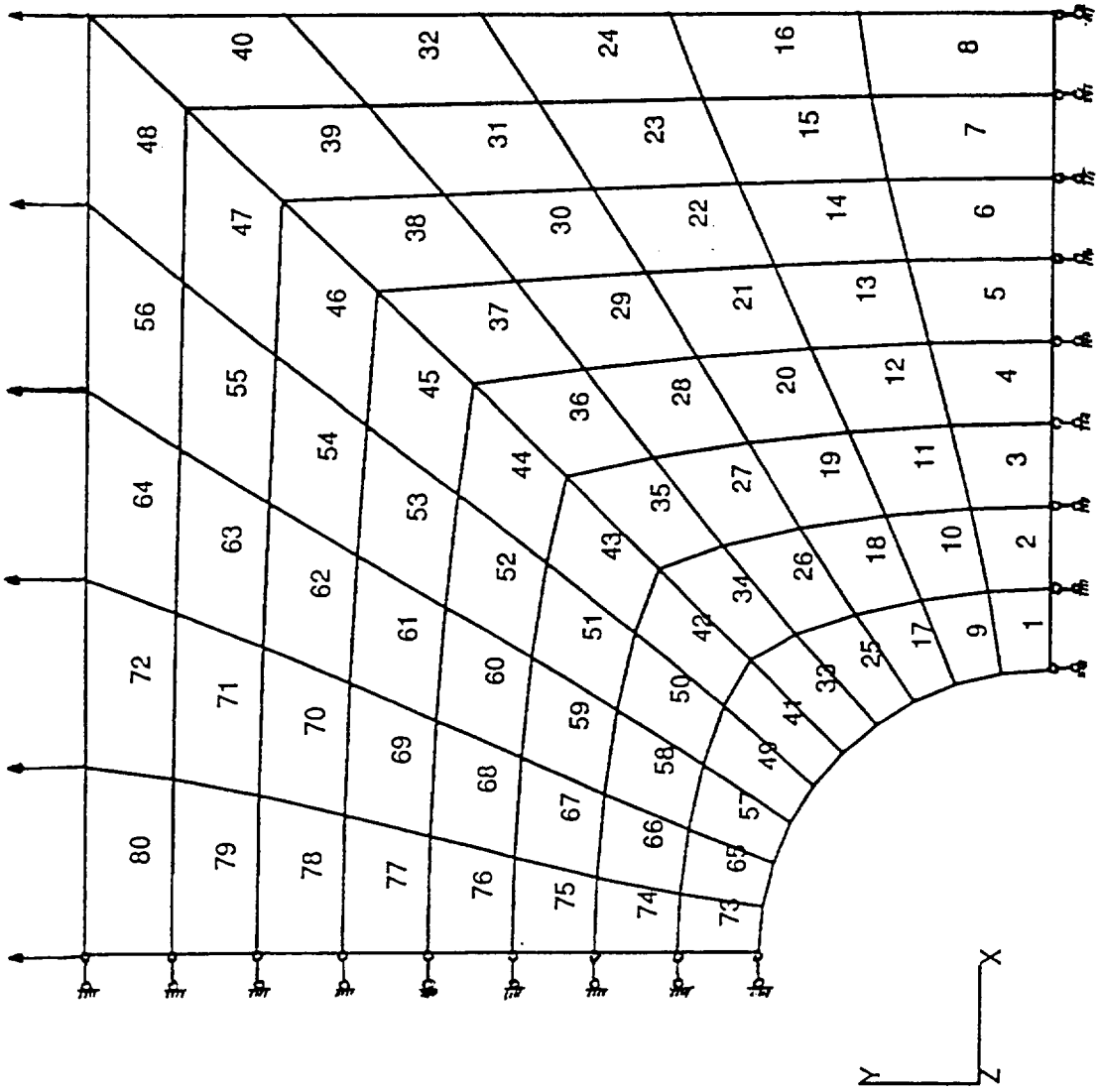

Figure 16 Structure mesh

final load level when 1, 5 and 20 global steps are utilized respectively. Also in order to check the convergence and efficiency of the implicit integration scheme, an explicit test is run by using 5000 global steps as the reference solution. The result shown in Figure 20 and Figure 21 are the effective inelastic strain distribution at the final load level by using the implicit scheme (20 global steps) and explicit scheme (5000 global steps), respectively. Note that the difference between these two figures is less than 1% which means the 20 step case converged and may be chosen as the reference solution. Comparing the 5 and 20 step cases (Figure 18 and 19), note that the effective stress distribution of the 5 step case is qualitatively close to the 20 step case which shows reasonable accuracy for even the 5 step case. Also, convergence was achieved using only one global step, this demonstrates the robustness of the implicit integration algorithm. Although the accuracy has decreased (12% difference in maximum J_2) which is understandable since this is a first order integration method and just one step is used. The CPU time for the explicit scheme, and the 20, 5, and 1 step implicit cases are 12570, 251, 91 and 25 minutes, respectively. The CPU ratio of the explicit versus the implicit scheme (20 steps) is more than 50, thus showing the significant efficiency of the implicit integration scheme. Comparing the implicit scheme itself, the CPU ratio of the 20 step case to that of the 5 step case is approximately 2.7. This a significant saving in computation time yet the results are almost identical, i.e. the difference is less than 2%. Thus, for the complex structural problem, convergence may be reached in an efficient manner without a significant loss in accuracy. Again, there will always be a balance between solution accuracy and computational efficiency.

5. Summary & Conclusions

The general computational framework described in this report using the backward Euler fully-implicit integration method has been determined to be successful for both the

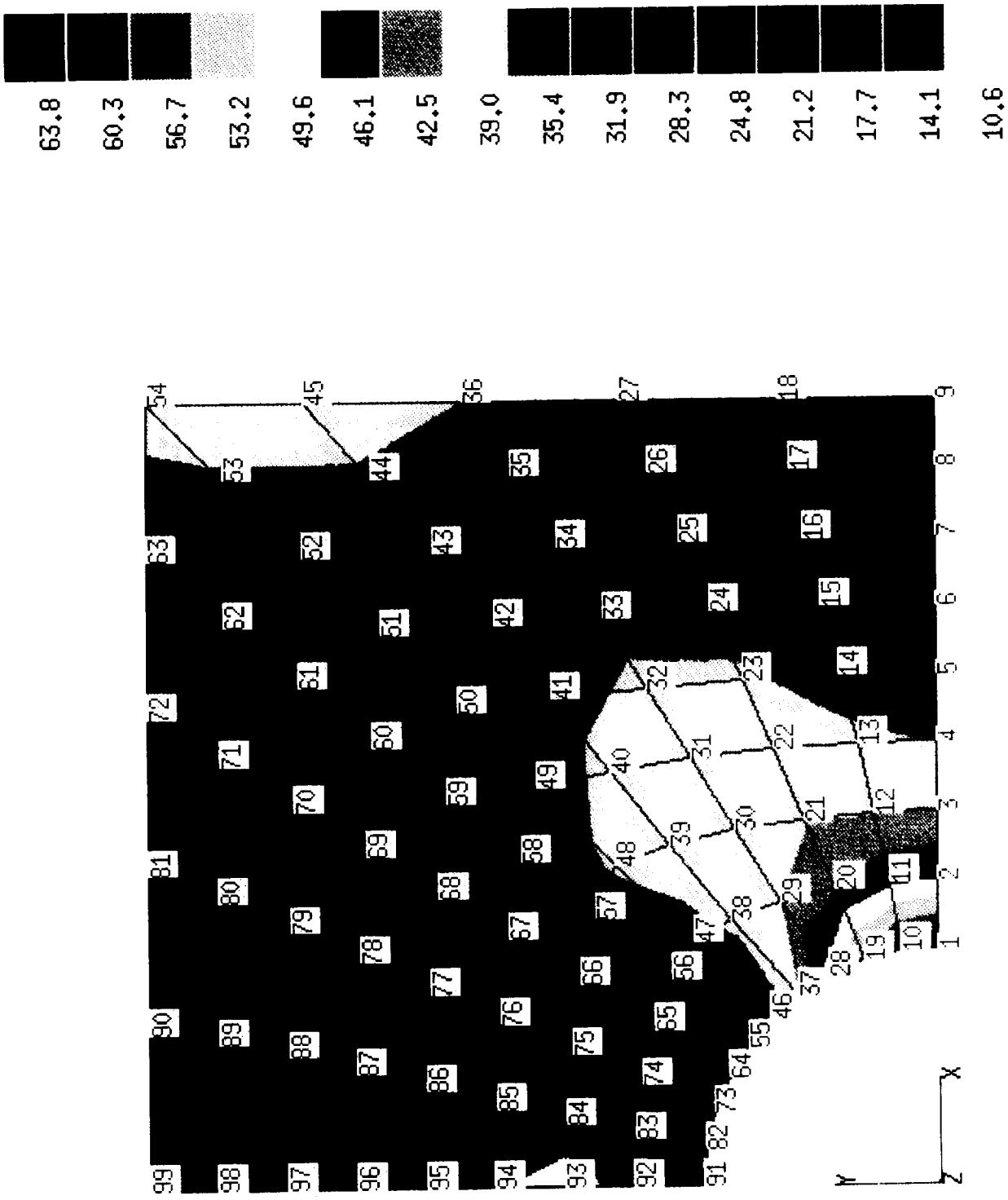

Figure 17 Effective stress distribution (1 step)

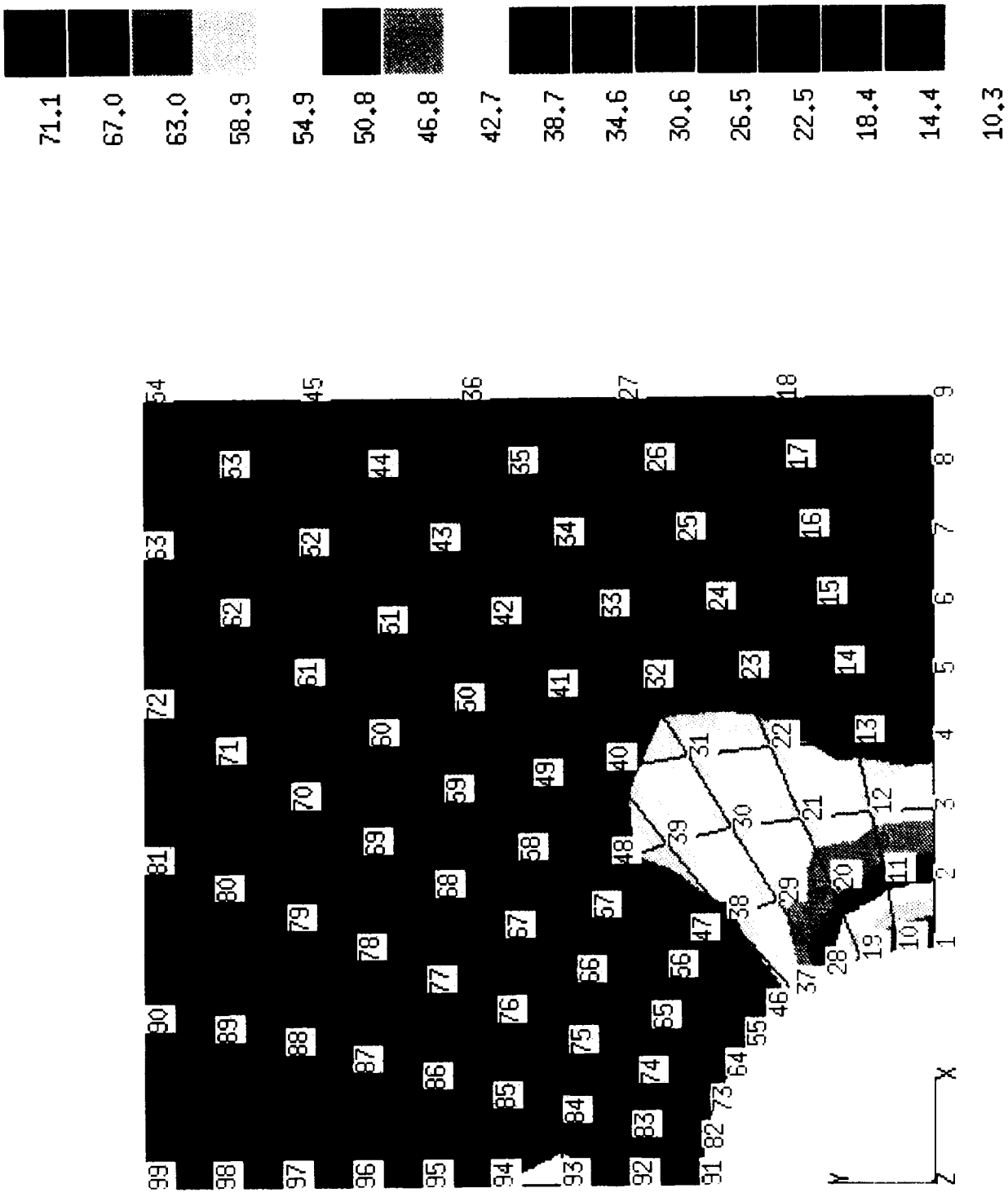

Figure 18 Effective stress distribution (5 steps)

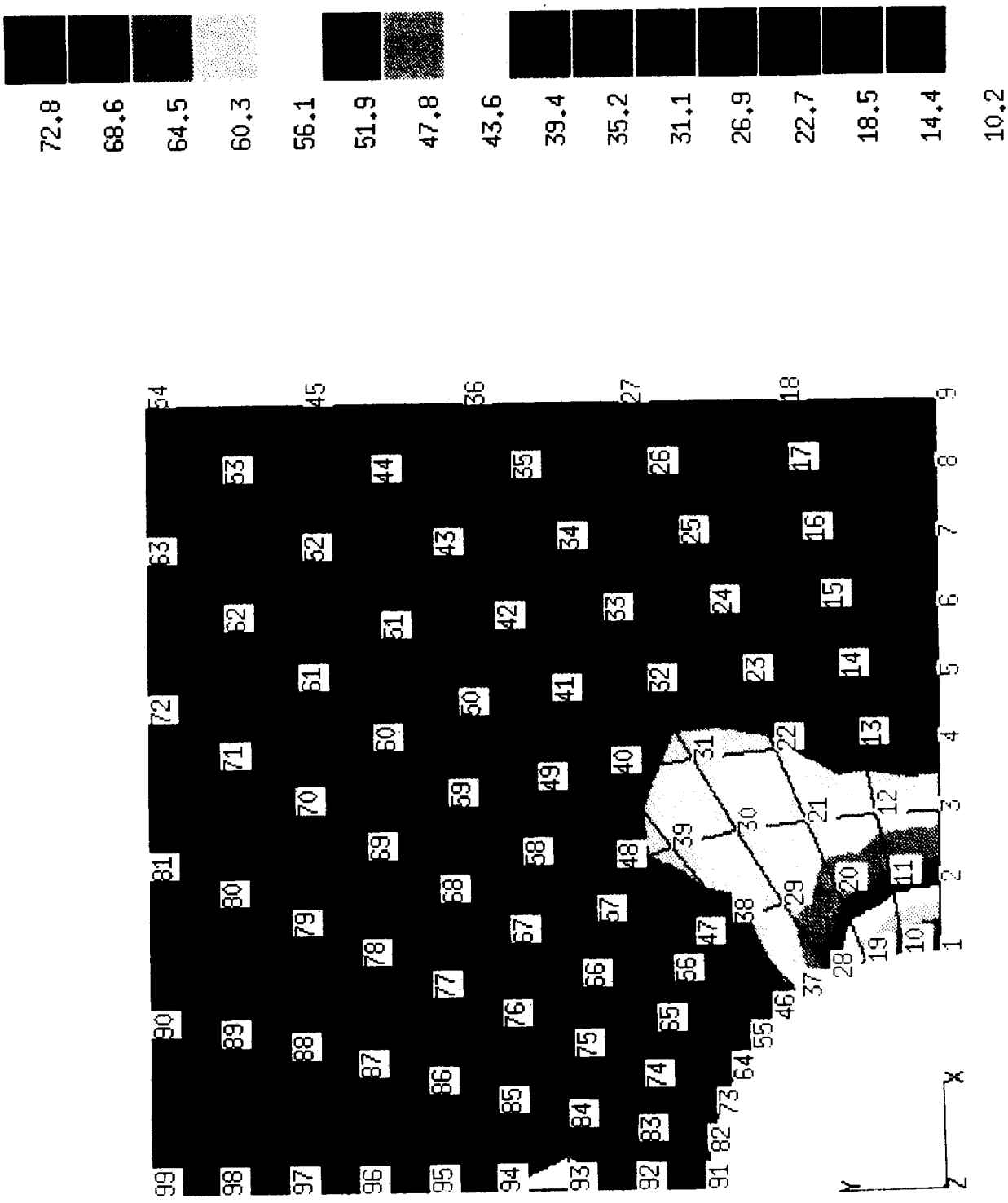

Figure 19 Effective stress distribution (20 steps)

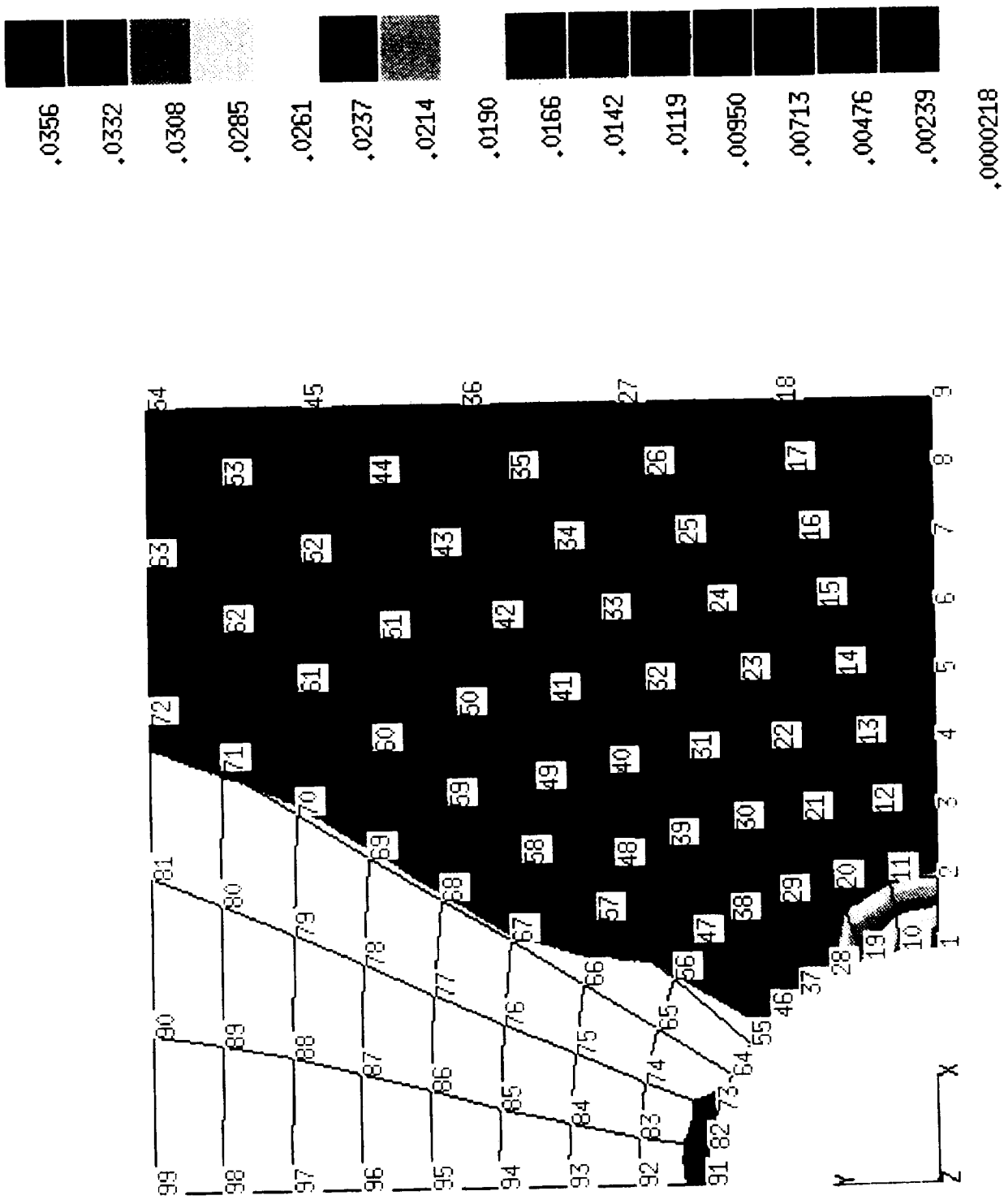

Figure 20 Effective inelastic strain distribution (20 steps)

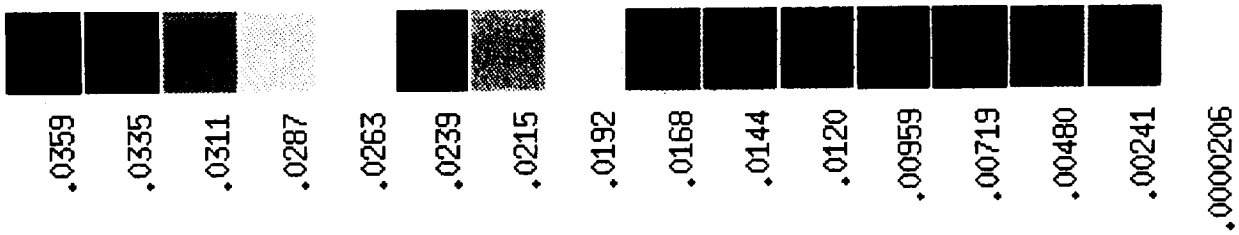

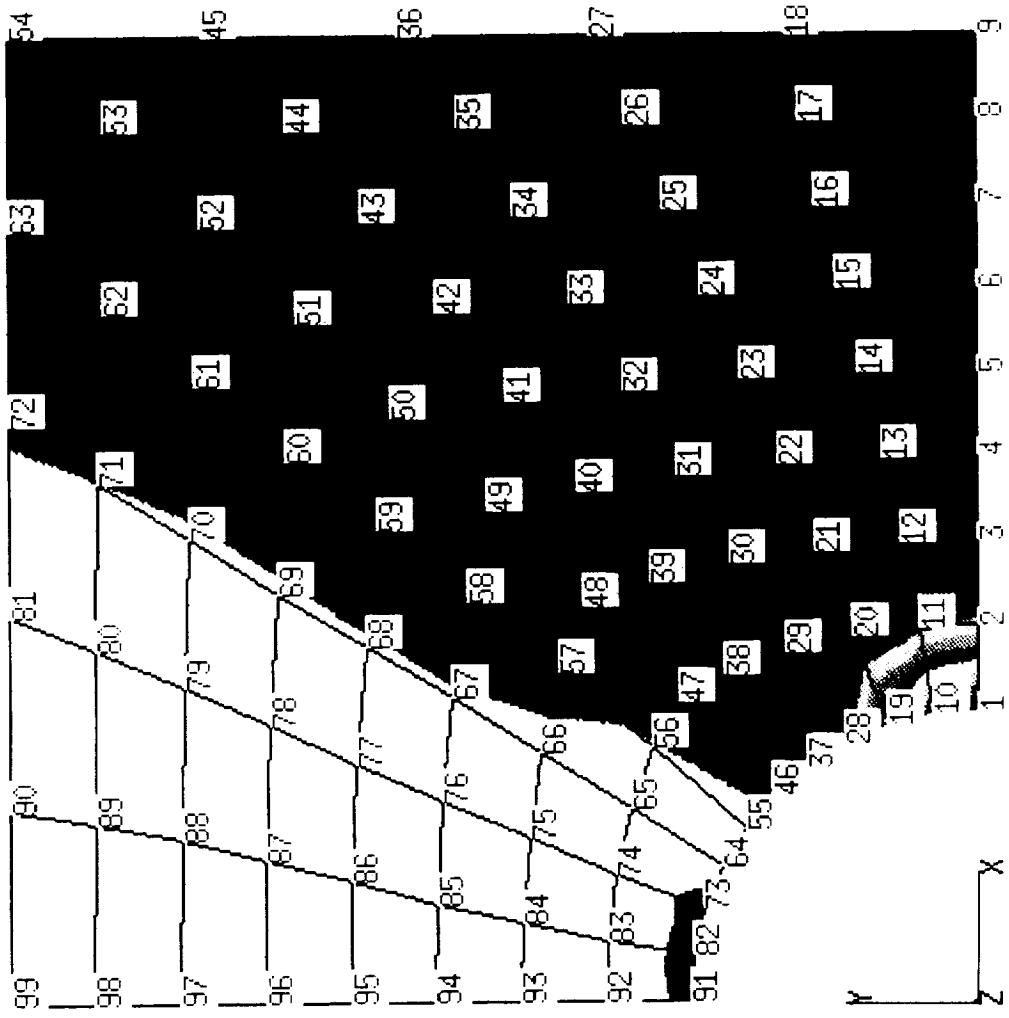

Figure 21 Effective inelastic strain distribution (5000 steps, explicit method)

Generalized Viscoplasticity with Potential Structure (GVIPS) and the Non-Associative Viscoplastic models (NAV). Only these Newton iterative schemes will provide, uniformly-valid, convergent, implicit integrations for both GVIPS and NAV classes of viscoplastic models. The algorithm was written in a concise matrix format so as to provide sufficient generality and is automatically valid for both isotropic and anisotropic cases in full space or subspaces.

All numerical tests show that the use of the implicit integration method is robust, unconditionally-stable and provides first-order accuracy for both "small" and "large" Δt that is, the integration method provides a balanced combination of stability and accuracy. Even with nonproportional, multiaxial stress-strain states, sufficient accuracy and good convergence characteristics were demonstrated for the implemented scheme.

In addition, it has been generally observed that explicit schemes either fail completely or become prohibitively expensive, especially for the NAV class of models. Specifically the time step size must be inherently very small in order to guarantee convergence, which is not efficient. It is believed that this point has been clearly demonstrated in the results presented here for the explicit integration cases. That is, it was required that the number of time steps be on the order of 10,000 to 80,000 in order to obtain a solution. These results appear to be consistent with other recent work, for example that of Arya [7], that uses various explicit schemes.

The implicit integration scheme with simple subincrementing, which improves convergence, has been shown to be efficient when used for GVIPS and NAV. But on the other hand, subincrementing alone is not efficient. That is, many subincrements and local iterations are required. As a result, the "slack" method, which is the form of line search in the present algorithm, enables the NAV class of models to converge stably with sufficient accuracy and significantly improved efficiency.

In comparing the recently-developed GVIPS class model versus some forms of the presently-used NAV models found in the literature, the GVIPS formulation posses a more theoretically sound basis from the thermodynamics standpoint, and exhibit symmetries which are desirable with respect to computation in the corresponding integrated forms of their flow and evolution equations. For example, for global iterations, GVIPS provide a fully-consistent tangent stiffness, but for NAV, only an approximate tangent stiffness is obtained. From the numerical tests in this report, it was found that NAV exhibited greater difficulty in integration when compared to the GVIPS model. That is, NAV required more iterations in order to reach a solution. However, by means of a line search scheme, NAV (because of its continuous formulation), can now be integrated more easily even without subincrementing. The overall efficiency of integrating the GVIPS class of viscoplastic models is even more impressive when one recalls that a combination of subincrementing and line search methods must be applied; because of the discontinuity in GVIPS evolution equations, due to the need to correctly account for unloading. In particular, in the discontinuous regions, subincrementing is still required to refine the time steps sufficiently in order to capture the discontinuity, but is only needed in those areas (few steps) near the discontinuity. Alternatively, in the continuous regions, of GVIPS the use of a line search technique applies and does contribute significantly to improve convergence. Thus, intelligent combination of line search and subincrementing guidance convergence as well as overall efficiency for the GVIPS class of models.

Appendix 1: Material constants

NAV material constants (Copper):

Constant	Value	Units
T_t	678	K
μ_0	43000	MPa
μ_1	-17	MPa/K
h_0	50	MPa
h_1	15	MPa
Q	200,000	J/mol.
K	8.314	J/mol. K
A	20,000,000	1/s
n	4.5	
C	13	MPa
D_0	0.13	MPa
f	0.75	
δ	0.035	
m	0.5	
H_0	20	
ν	0.36	

GVIPS material constants (W/Kanthal):

Constant	Value	Units
n	1.5	
μ	2.5E4	hr
m	1.5	
β	0.5	
R	7.0E-5	MPa/hr
H	12.6E4	MPa
G_0	0.05	
ω	2.7	
η	1.0	
k_t	5.6	MPa

Appendix 2: Modified material constants

GVIPS material constants for nonproportional test:

Constant	Value	Units
n	2.5	
μ	8.1238E12	hr
m	3.0	
β	2.5	
R	7.0E-4	MPa/hr
H	2.0E4	MPa
G_0	2.5	
ω	1.0	
η	1.0	
k_t	0.6823	MPa

REFERENCES

1. Agarwal, B.D., and Broutman, L.J., "Analysis and Performance of Fiber Composites", John Wiley and Sons, 1980.

2. Argyris, J.H., Vaz, L.E., and Willam, K. J. , "Improved Solution Methods for Inelastic Rate Problems", *Comp. Meth. in Appl. Mech. Eng.*, Vol. 16, pp. 231-277, 1978.

3. Arnold, S. and Saleeb, A.F., "On the Thermodynamic Framework of Generalized, Coupled Thermoelastic-Viscoplastic-Damage Modeling", Int. J. Plasticity,Vol. 10, No. 3, pp. 263-278, 1994.

4. Arnold, S. M., Saleeb, A. F. and Castelli, M. G., " A Fully Associative, Non-linear Kinematic, Unified Viscoplastic Model for Titanium Based Matrices", NASA TM-106609, NASA Lewis Research Center, OH, 1994.

5. Arnold, S. M., Saleeb, A. F. and Wilt, T. E., "A Modeling Investigation of Thermal and Strain Induced Recovery and Nonlinear Hardening in Potential Based Viscoplasticity", NASA TM-106122, NASA Lewis Research Center, OH, 1993.

6. Arnold, S.M., "A Transversely Isotropic Thermoelastic Theory", NASA TM101302, NASA Lewis, Ohio, 1989.

7. Arya, V. K., "Efficient and Accurate Explicit Integration Algorithms with Application to Viscoplastic Models", NASA CR 195342, 1994.

8. Arya, V.K., and Kaufman, A., "Finite Element Implementation of Robinson's Unified Viscoplastic Model and Its Application to Some Uniaxial and Multiaxial Problems", *Eng. Comput.*, Vol. 6, pp. 237-248, 1989.

9. Bahei-El-Din, Y.A., and Dvorak, G.J., "Plasticity Analysis of Laminated Composite Plates", *J. Appl. Mech.*, ASME, Vol. 49, pp. 740-746, 1982.

10. Bahei-El-Din, Y.A., Dvorak, G.J., and Utku, S., "Finite Element Analysis of Elastic-Plastic Fibrous Composite Structures", *Computers and Structures*, Vol. 13, pp. 321-330, 1981.

11. Bird, W.W. and Martin, J.B., "Consistent Predictors and the Solution of the Piecewise Holonomic Incremental Problem in Elastoplasticity", *Eng. Struct.* 12, 9-14, 1990.

12. Boisse, P., Bussy, P., and Ladeveze, P., "A New Approach in Nonlinear Mechanics: the Large Time Increment Method", *Int. J. Num. Meth. Eng.*, Vol. 29, pp. 647-663, 1990.

13. Brockman, R.A., "Explicit Forms For The Tangent Modulus Tensor In Viscoplastic Stress Analysis", *Int. J. Number. Meth. Engng.*, Vol. 20, pp. 315-319, 1984.

14. Caddemi, S., and Martin, J.B., "Convergence of the Newton-Raphson Algorithm in Elastic-Plastic Incremental Analysis", *Int. J. Num. Meth. Eng.*, Vol. 31, pp. 177-191, 1991.

15. Chaboche, J. L., "Constitutive Equations for Cyclic Plasticity and Cyclic Viscoplasticity", Int. J. Plasticity, Vol. 5, pp.247-302, 1989.

16. Chang, T.Y., Chen, J.Y., and Chu, S.C., "Viscoplastic Finite Element Analysis By Automatic Subincrementing Technique", *ASCE J. of Eng. Mech.*, Vol. 114, pp. 80-96, 1988.

17. Chuyla, A., and Walker, K.P., "A New Uniformly Valid Asymptotic Integration Algorithm for Elasto-Plastic-Creep and Unified Viscoplastic Theories Including Continuum Damage", NASA TM 102344, December 1989.

18. Cohn, M.Z., and Maier, G. (eds.), *Engineering Plasticity by Mathematical Programming*, Pergamon Press, Oxford, 1979.

19. Coleman, B.D., and Gurtin, M.E., "Thermodynamics with Internal State Variables", *J. Chem. Phys.*, Vol. 47, 1967, pp. 597-613.

20. Crisfield, M. A., *Nonlinear Finite Element Method of the Structure and Solids*, Chichester, New York, Wiley, 1991

21. DeBorst, R. and Feenstra, P.H., "Studies in Anisotropic Plasticity with Reference to the Hill Criterion", *Int.J. Num. Meth. in Eng.*, Vol. 29, pp. 315-336, 1990.

22. Dodds, R.H., Jr., "Numerical Techniques for Plasticity Computations in Finite Element Analysis", *Comput. and Struct.*, Vol. 26, pp. 767-779, 1987.

23. Ekeland, I., and Teman, R., *Convex Analysis and Variational Problems*, North-Holland, Amsterdam, 1976.

24. Freed, A. D. and Walker, K. P., "Viscoplasticity with Creep and Plasticity Bounds", Int. J. Plasticity, Vol. 9, 213-242, 1993.

25. Freed, A.D. and Walker, K.P., "Refinements in a Viscoplastic Model", NASA TM-102338, NASA Lewis Research Center, OH, 1989.

26. Gear, G.W., *Numerical Initial Value Problems in Ordinary Differential Equations*, Prentice-Hall, Inc., New Jersey, 1971.

27. Haslach, H. W., Freed, A. D. and Walker, K. P., *Non-Linear Asymptotic Integration Algorithms for Two Dimensional Autonomous Dissipative First-Order ODEs*, to appear as NASA TM, NASA Lewis, 1995.

28. Hill, R., *The Mathematical Theory of Plasticity*, Clarendon Press, Oxford, 1950.

29. Hornberger, K., and Stamm, H., "An Implicit Integration Algorithm with a Projection Method for Viscoplastic Constitutive Equations", *Int. J. Number. Meth. Engng.*, Vol. 28, pp. 2397-2421, 1989.

30. Hughes, T.J.R., and Taylor, R.L., "Unconditionally Stable Algorithms, for Quasistatic-Viscoplastic Finite Element Analysis", *Comp. and Struct.*, Vol. 8, pp. 169-173, 1978.

31. Jetteur, P., "Implicit Integration Algorithm for Elastoplasticity in Plane Stress Analysis", *Eng. Comp.*, Vol. 3, pp. 251-258, 1986.

32. Johnson, C., "On Plasticity with Hardening", *J. Appl. Math. Anal.*, Vol. 62, pp. 325-336, 1978.

33. Ju, J.W., "Consistent Tangent Moduli for a Class of Viscoplasticity", *J. Engng. Mech.*, ASCE, Vol. 116, pp. 1704-1779, 1990.

34. Krieg, R.D. and Krieg, D.B., "Accuracies of numerical solution methods for the elastic perfectly plastic model", *ASME Journal of Pressure Vessel Technology*, 99, 510-515 (1977).

35. Kumar, V., Morjaria, M., and Mukherjee, S., "Numerical Integration of Some Stiff Models of Inelastic Deformations", *J. Eng. Mat. and Tech.*, ASME, Vol. 102, pp. 91-96, 1980.

36. Lamba, H. S. and Sidebottom, O. M., "Cyclic Plasticity for Nonproportional Paths", Part I, II, J. of Engn. Materials and Tech., vol 100, pp. 93-111, 1978

37. Lemaitre, J. and Chaboche, J.L., *Mechanics of Solid Materials*, Cambridge University Press, N.Y., 1990.

38. Li, W. and Saleeb, A. F., "Robust integration Schemes for Generalized Viscoplasticity with Internal-State Variables", Part II, NASA CR195453, 1995

39. Lubliner, J., "On the Structure of the Rate Equations of Materials with Internal Variables", *Acta Mech.*, 17, 1973, pp. 109-119.

40. Lush, A.M., Weber, G., and Anand, L., "An Implicit Time-Integration Procedure for a Set of Internal Variable Constitutive Equations for Isotropic Elasto-Viscoplasticity", 5(5), pp. 521-549, 1987.

41. Maier, G. and Novati, G., "Extremum Theorems for Finite Step Backward Difference Analysis of Elastic Plastic Nonlinearly Hardening Solids", *Int. J. Plasticity*, Vol. 6, pp. 1-10, 1990.

42. Marques, J.M.M.C., Owen, D.R.J., "Strain Hardening Representation For Implicit Quasistatic Elasto-Viscoplastic Algorithms", *Comput. Struct.*, Vol. 17, pp. 301-304, 1983.

43. Martin, J.B., Reddy, B.D., Griffin, TB., and Bird, W.W., "Applications of Mathematical Programming Concepts to Incremental Elastic-Plastic Analysis, *Eng. Struct.*, 9, 171-176, 1987.

44. Miller, A.K., and Tanaka, T.G., "NONSS: A New Method for Integrating Unified Constitutive Equations Under Complex Histories", *J. Eng. Mat. Tech.*, ASME, Vol. 110, pp. 205-211, 1988.

45. Moran, B., Ortiz, M., and Shih, F., "Formulation of Implicit Finite Element Methods for Multiplicative Finite Deformation Plasticity", *Int. J. Num. Meth. Eng.*, Vol. 29, pp. 483-514, 1990.

46. Moreau, J.J., "Evolution Problem Associated with a Moving Convex Set in a Hilbert Space", *J. Diff. Eqn.*, Vol. 26, pp. 347-353, 1977.

47. Musgrave, M.J.P., *Crystal Acoustics*, Holden-Day, San Francisco, 1970.

48. Nagtegaal, J.C., "On the Implementation of Inelastic Constitutive Equations with Special Reference to Large Deformation Problems", *Comp. Meth. Appl. Mech. Eng.*, Vol. 33, pp. 469-484, 1982.

49. Nayak, G.C. and Zienkiewicz, O.C., "Elasto-plastic stress analysis: a generalization for various constitutive laws including strain softening", *Int. J. Number. Methods Eng.*, 5, 113-135 (1972).

50. Nguyen, Q.S., "On the Elastic-Plastic Initial Boundary Value Problem and its Numerical Integration", *Int. J. Num. Meth. Eng.*, Vol. 11, pp. 817-832, 1977.

51. Ortiz, M., and Popv, E.P., "Accuracy and Stability of Integration Algorithms for Elastoplastic Constitutive Relations", *Int. J. Num. Meth. Eng.*, Vol 21, pp. 1561-1576, 1985.

52. Ortiz, M., and Simo, J.C., "An analysis of a New Class of Integration Algorithms for Elastoplastic Constitutive Relations", *Int. J. Num. Meth. Eng.*, Vol. 23, pp. 353-366, 1986.

53. Owen D.R.J., and Liu, G.Q., "Elasto-Viscoplastic Analysis of Anisotropic Laminated Plates and Shells", *Eng. Comput.*, Vol. 2, n. 2, pp. 90-95, 1985.

54. Owen, D.R.J. and Hinton, E., *Finite Elements in Plasticity: Theory and Practice*, Pineridge Press, Swansea, U.K., 1980.

55. Owen, D.R.J., and Figueiras, J.A., "Anisotropic Elasto-Plastic Finite Element Analysis of Thick and Thin Plates", *Int. J. Number. Meth. Eng*, Vol. 19, pp. 541-566, 1983.

56. Owen, D.R.J., and Figueiras, J.A., "Elasto-Plastic Analysis of Anisotropic Plates and Shells by the Semiloof Element", *Int. J. Number. Meth. Eng.*, Vol. 19, pp. 521-539, 1983.

57. Pierce, D., Shih, C.F., and Needleman, A., "A Tangent Modulus Method For Rate Dependent Solids", *Comput. Struct.*, Vol. 18, pp. 875-887, 1984.

58. Prezyna, P., "Thermodynamic Theory of Viscoplasticity", in *Advances in Applied Mechanics*, Vol. 11, Academic Press, New York, 1971.

59. Riggs, H.R., "A Substructure Analogy for Plasticity", *Comput. and Struct.*, Vol. 37, pp. 405-412, 1990.

60. Robinson, D.N., and Duffy, S.F., "Continuum Deformation Theory for High-Temperature Metallic Composites", *J. Eng. Mech.*, ASCE, Vol. 116, No. 4, pp. 832-844, 1990.

61. Robinson, D.N., Binienda, W.K., and Miti-Kavuma, M., "Creep and Creep Rupture of Strongly Reinforced Metallic Composites", *J. Eng. Mech.*, ASCE, Vol. 118, No. 8, pp. 1646-1660, 1992.

62. Robinson, D.N., Duffy, S.F. and Ellis, J.R., "A Viscoplastic Constitutive Theory for Metal-Matrix Composites at High-Temperature", in *Thermal Stress, Material Deformation, and Thermomechanical Fatigue*, H. Sehitoglu and S.Y. Zamrik (eds., ASME-PVP, New York, Vol. 123, pp. 49-56, 1987.

63. Runesson, K., Samuelsson, A., and Bernspang, L., "Numerical Techniques in Plasticity Including Solution Advancement Control", *Int. J. Num. Meth. Eng.*, Vol. 22, pp. 769-788, 1986.

64. Runesson, K., Sture, S., and Willam, K., "Integration in Computational Plasticity", *Comput. and Struct.*, Vol. 30, pp. 119-130, 1988.

65. Saleeb, A. F. and Wilt, T. E.," Analysis of theAnisotropic Viscoplastic-Damage Response of Composite Laminates-Continuum Basis and Computational Algorithm", *Int. J. Num. Meth. Eng.*, Vol. 36, 1629-1660 (1993).

66. Saleeb, A.F., Chang, T.Y., Graf, W., and Yingyeunyong, S., "A Hybrid/Mixed Model for Nonlinear Shell Analysis and its Applications to Large Rotation Problems", *Int. J. Num. Meth. Eng.*, Vol. 29, pp. 407-446, 1990.

67. Schreyer, H.L., Kulak, R.F., and Kramer, J.M. "Accurate Numerical Solutions for Elasto-plastic Models", *ASME Journal of Pressure Vessel Technology*, 101, 226-234 (1979).

68. Simo, J.C. and Taylor, R.L., "A Return Mapping Algorithm for Plane Stress Elastoplasticity", *Int. J. Num. Meth. Eng.*, Vol. 22, pp. 649-670, 1986.

69. Simo, J.C., and Taylor, R.L., "Consistent Tangent Operators for Rate-Independent Elastoplasticity", *Comp. Meth. Appl. Mech. Eng.*, Vol. 48, pp. 101-118, 1985.

70. Sotolongo, W., and McDowell, D.L., "On the Numerical Integration of Elastoplastic Constitutive Model Structures for Nonproportional Cyclic Loading", *Comput. and Struct.*, Vol.24, pp. 595-606, 1986.

71. Spencer, A.J.M. (editor), *Continuum Theory of the Mechanics of Fiber-Reinforced Composites*, Springer-Verlag, New York, 1984.

72. Spencer, A.J.M., *Deformations of Fiber-Reinforced Materials*, Clarendon Press, Oxford, 1971.

73. Sutcliff, S., "Shear Modulus Bounds for Transverse Isotropy", in *Recent Advances in Engineering Mechanics and Their Impact on Civil Engineering Practice*, Vol. II, Chen, W.F., and Lewis, A.D. (eds.), ASCE, pp. 778-781, 1983.

74. Szabo, L., "Tangent Modulus Tensors For Elastic-Viscoplastic Solids", *Comput. Struct.*, Vol. 34, pp. 401-419, 1990.

75. Walker, K.P., and Freed, A.D., "Asymptotic Integration Algorithms for Nonhomogeneous, Nonlinear, First Order, Ordinary Differential Equations", NASA TM-103793, NASA Lewis Research Center, OH, 1991; also *J. Comp. Phys.* (to appear).

76. Waltz, G., Hornberger, K., and Stamm, H., "An Implicit Integration Algorithm for Plane Stress Viscoplastic Constitutive Equations", *Computers and Structures*, Vol. 36, pp. 539-546, 1990.

77. Whirley, R.G., Hallquist, J.O., and Goudreau, G.L., "An Assessment of Numerical Algorithms for Plane Stress and Shell Elastoplasticity on Supercomputers", *Eng. Comput.*, Vol. 6, pp. 116-126, 1989.

78. Willam, K.J., "Numerical Solution of Inelastic Rate Processes", *Computers and Structures*, Vol. 8, pp. 511-531, 1978.

79. Wilt, T.E., Saleeb, A.F., and Chang, T.Y.P., "A Mixed Element for Plates and Shells", *Comput. and Struct.*, Vol. 37, pp. 597-612, 1990.

80. Zienkiewicz, O.C., and Cormeau, I.C., "Viscoplasticity-Plasticity and Creep in Elastic Solids – A Unified Approach", *Int. J. Number. Meth. Engng.*, Vol. 8, pp. 821-845, 1974.

REPORT DOCUMENTATION PAGE

Form Approved
OMB No. 0704-0188

1. AGENCY USE ONLY (*Leave blank*)	2. REPORT DATE	3. REPORT TYPE AND DATES COVERED
	May 1995	Final Contractor Report

4. TITLE AND SUBTITLE

Robust Integration Schemes for Generalized Viscoplasticity With Internal-State Variables

Part I Theoretical Developments and Applications

5. FUNDING NUMBERS

WU-505-63-5B
G-NAG3-1493

6. AUTHOR(S)

Atef F. Saleeb and Wei Li

7. PERFORMING ORGANIZATION NAME(S) AND ADDRESS(ES)

University of Akron
Akron, Ohio 44325-3905

8. PERFORMING ORGANIZATION REPORT NUMBER

E-9534

9. SPONSORING/MONITORING AGENCY NAME(S) AND ADDRESS(ES)

National Aeronautics and Space Administration
Lewis Research Center
Cleveland, Ohio 44135-3191

10. SPONSORING/MONITORING AGENCY REPORT NUMBER

NASA CR-195452

11. SUPPLEMENTARY NOTES

Project Manager, S.M. Arnold, Structures Division, NASA Lewis Research Center, organization code 5220, (216) 433-3334.

12a. DISTRIBUTION/AVAILABILITY STATEMENT

Unclassified - Unlimited
Subject Category 39

This publication is available from the NASA Center for Aerospace Information, (301) 621-0390.

12b. DISTRIBUTION CODE

13. ABSTRACT ***(Maximum 200 words)***

This two-part report is concerned with the development of a general framework for the implicit time-stepping integrators for the flow and evolution equations in generalized viscoplastic models. The primary goal is to present a complete theoretical formulation, and to address in detail the algorithmic and numerical analysis aspects involved in its finite element implementation, as well as to critically assess the numerical performance of the developed schemes in a comprehensive set of test cases. On the theoretical side, the general framework is developed on the basis of the unconditionally-stable, backward-Euler difference scheme as a starting point. Its mathematical structure is of sufficient generality to allow a unified treatment of different classes of viscoplastic models with internal variables. In particular, two specific models of this type, which are representative of the present start-of-art in metal viscoplasticity, are considered in applications reported here; i.e., fully associative (GVIPS) and non-associative (NAV) models. The matrix forms developed for both these models are directly applicable for both initially isotropic and anisotropic materials, in general (three-dimensional) situations as well as subspace applications (i.e., plane stress/strain, axisymmetric, generalized plane stress in shells). On the computational side, issues related to efficiency and robustness are emphasized in developing the (local) interative algorithm. In particular, closed-form expressions for residual vectors and (consistent) material tangent stiffness arrays are given explicitly for both GVIPS and NAV models, with their maximum sizes "optimized" to depend only on the number of independent stress components (but independent of the number of viscoplastic internal state parameters). Significant robustness of the local iterative solution is provided by complementing the basic Newton-Raphson scheme with a line-search strategy for convergence. In the present first part of the report, we focus on the theoretical developments, and discussions of the results of numerical-performance studies using the integration schemes for GVIPS and NAV models.

14. SUBJECT TERMS	15. NUMBER OF PAGES
Viscoplasticity; Multiaxial; Numerical integration; Finite element; Implicit; Line search; Algorithm, Anisotropic; Isotropic	84
	16. PRICE CODE: A05

17. SECURITY CLASSIFICATION OF REPORT	18. SECURITY CLASSIFICATION OF THIS PAGE	19. SECURITY CLASSIFICATION OF ABSTRACT	20. LIMITATION OF ABSTRACT
Unclassified	Unclassified	Unclassified	

National Aeronautics and
Space Administration

Lewis Research Center
21000 Brookpark Rd.
Cleveland, OH 44135-3191